DOI: 10.1534/genetics.110.120766

System-Level Analysis of Genes and Functions Affecting Survival During Nutrient Starvation in *Saccharomyces cerevisiae*

David Gresham,*[,1] Viktor M. Boer,[†,2] Amy Caudy,[†] Naomi Ziv,* Nathan J. Brandt,* John D. Storey[†,‡] and David Botstein[†,‡,1]

**Department of Biology, Center for Genomics and Systems Biology, New York University, New York, New York 10003 [†]The Lewis-Sigler Institute for Integrative Genomics and [‡]Department of Molecular Biology, Princeton University, Princeton, New Jersey 08544*

Manuscript received July 10, 2010
Accepted for publication September 28, 2010

ABSTRACT

An essential property of all cells is the ability to exit from active cell division and persist in a quiescent state. For single-celled microbes this primarily occurs in response to nutrient deprivation. We studied the genetic requirements for survival of *Saccharomyces cerevisiae* when starved for either of two nutrients: phosphate or leucine. We measured the survival of nearly all nonessential haploid null yeast mutants in mixed populations using a quantitative sequencing method that estimates the abundance of each mutant on the basis of frequency of unique molecular barcodes. Starvation for phosphate results in a population half-life of 337 hr whereas starvation for leucine results in a half-life of 27.7 hr. To measure survival of individual mutants in each population we developed a statistical framework that accounts for the multiple sources of experimental variation. From the identities of the genes in which mutations strongly affect survival, we identify genetic evidence for several cellular processes affecting survival during nutrient starvation, including autophagy, chromatin remodeling, mRNA processing, and cytoskeleton function. In addition, we found evidence that mitochondrial and peroxisome function is required for survival. Our experimental and analytical methods represent an efficient and quantitative approach to characterizing genetic functions and networks with unprecedented resolution and identified genotype-by-environment interactions that have important implications for interpretation of studies of aging and quiescence in yeast.

THE normal life of most cells comprises alternating periods of growth and quiescence. Commitment to the mitotic cell cycle represents a critical decision for a cell and requires mechanisms for determining that internal and external conditions are sufficient to ensure successful traversal of the cell division cycle. The application of genetic approaches to the study of the cell division cycle in the model organisms *Saccharomyces cerevisiae* (budding yeast) and *Schizosaccharomyces pombe* (fission yeast) yielded a detailed understanding of the molecular processes underlying progression of the cell division cycle (Hartwell *et al.* 1974; Nurse 1975; Johnston *et al.* 1977). Subsequent work showed that the major molecules and principles of cell division are conserved from yeast to humans and that dysregulation of the cell cycle is a hallmark of cancers (Hartwell 1991, 2002; Nurse *et al.* 1998; Nurse 2002). By contrast with our understanding of the mitotic cell cycle, our knowledge of the molecular processes that govern exit from the cell cycle and prolonged maintenance of a viable nonproliferative cellular state in both humans and model systems is poor. A detailed understanding of the molecular mechanisms mediating cell cycle exit and maintenance of a viable quiescent state is critical to understanding normally functioning cells, which are primarily postmitotic, and their aberrant states.

Yeast cells cease active cell division when external conditions are unfavorable for continued growth (Johnston *et al.* 1977; Lillie and Pringle 1980). The extracellular status of compounds containing essential elements such as carbon, sulfur, nitrogen, and phosphorus is particularly important and when these elements are in low abundance cells exit the cell cycle. Specialized sensing mechanisms appear to uniquely determine the status of different essential nutrients and connect to signaling pathways such as the RAS/protein kinase A (PKA) and TOR pathways that mediate myriad downstream effects affecting the transcriptional, translational, and metabolic state of the cell (Zaman *et al.* 2008). Remarkably, the different environmental signals result in the identical outcome: arrest in the G_0/G_1 stage of the cell division cycle. In yeast, exit from the

Supporting information is available online at http://www.genetics.org/cgi/content/full/genetics.110.120766/DC1.

Raw data are available at http://genomics-pubs.princeton.edu/StarvationGenetics/ and have been submitted to the NCBI Sequence Read Archive (http://www.ncbi.nlm.nih.gov/sra) under accession number SRA028412.1

[1]*Corresponding authors:* Center for Genomics and Systems Biology, Department of Biology, 100 Washington Square E., 1009 Silver Center, New York, NY 10003. E-mail: dgresham@nyu.edu; and The Lewis-Sigler Institute for Integrative Genomics, Princeton University, Princeton, NJ 08544. E-mail: botstein@genomics.princeton.edu

[2]*Present address:* DSM Food Specialties, Alexander Flemminglaan 1, 2613 AX Delft, The Netherlands.

cell cycle is associated with a number of physiological characteristics including increases in the carbohydrates trehalose and glycogen, a thickened cell wall, condensation of chromosomes, increased vacuolar volume, and increased resistance to stress (Werner-Washburne *et al.* 1993; Gray *et al.* 2004). Global studies have shown that cell cycle arrest associated with nutrient starvation is associated with dramatic alterations in transcript (Gasch *et al.* 2000; Saldanha *et al.* 2004; Brauer *et al.* 2005) and metabolite (Brauer *et al.* 2006) levels. Many of these changes appear to be consistent with an extrapolation of responses in transcript (Brauer *et al.* 2008) and metabolite (Boer *et al.* 2010) levels associated with decreasing growth rates, as determined in steady-state chemostat cultures. However, it remains unclear whether prolonged starvation results in a distinct cellular state (*i.e.*, a G_0 state) or whether cell cycle arrest is essentially identical to G_1 of the cell division cycle. Furthermore, it is unclear whether quiescent states induced by deprivation of different nutrients are equivalent.

The uniform cell cycle arrest initiated in response to starvation for nutrients such as carbon, phosphate, nitrogen, and sulfur is readily detected by the near complete absence of budded cells in the culture (Lillie and Pringle 1980). We previously referred to these nutrient conditions as "natural limitations" in contrast to "unnatural limitations," which can be imposed by starving an auxotrophic strain for its auxotrophic requirement (Saldanha *et al.* 2004). Importantly, in the case of unnatural limitations individual cells do not uniformly arrest as unbudded cells upon cessation of culture growth (Saldanha *et al.* 2004). Populations of prototrophic strains starved subjected to natural limitations maintain high viability for periods >100 days (Lillie and Pringle 1980). In contrast, starvation of an auxotrophic strain for its auxotrophic requirement results in dramatically reduced viability (Boer *et al.* 2008). Using a genetic selection, we previously showed that the poor survival of auxotrophs can be suppressed by loss-of-function mutations in the protein kinases *TOR1*, *SCH9*, and *PPM1*, a protein methyl transferase that regulates protein phosphatase 2A (Boer *et al.* 2008).

The survival of yeast cells during prolonged periods of starvation has also been used as a model of chronological aging of postmitotic cells (Fabrizio and Longo 2003). In studies that aim to use yeast as a model for this fundamental process the PKA and TOR pathways have been implicated in postmitotic aging in yeast (Fabrizio *et al.* 2001; Powers *et al.* 2006; Steffen *et al.* 2008; Burtner *et al.* 2009) and it has been argued that these same pathways underlie aging phenotypes in humans (Longo 2003). Although several of the loci identified in our original genetic screen (Boer *et al.* 2008) overlap with those identified in chronological aging studies (Fabrizio *et al.* 2001; Kaeberlein *et al.* 2005b; Powers *et al.* 2006), it has remained unclear whether mutations in these same components influence the survival of strains starved for naturally limiting nutrients such as sources of carbon, sulfur, nitrogen, and phosphorus.

To identify the genetic factors required for cell cycle exit and survival during prolonged nutrient starvation we performed complete screens of the 4811 haploid gene deletion mutants (Giaever *et al.* 2002) starved for two different nutrients. We performed this screen under conditions of phosphate starvation, a natural nutrient limitation, and leucine starvation, an unnatural nutrient limitation. Because our survival assay requires repeated measurements of viability over the period of starvation (Boer *et al.* 2008), the analysis of individual mutants is prohibitively time consuming and expensive. Therefore, we made use of the fact that each mutant is tagged by two unique molecular barcodes of 20-bp length that flank the antibiotic resistance cassette and can be amplified using common PCR priming sites (Giaever *et al.* 2002). Previously, multiplexed analysis of mutants was performed using DNA microarrays to assay the relative abundance of molecular barcodes as a means of estimating the abundance of each mutant (Giaever *et al.* 2002; Pierce *et al.* 2007; Yan *et al.* 2008; Ho *et al.* 2009). More recently, this approach was adapted to high-throughput sequence analysis (Smith *et al.* 2009). We independently developed a quantitative method using high-throughput sequencing of barcodes similar to that of Smith *et al.* (2009) for measuring the abundance of individual mutants in heterogeneous pools of mutants. We established a statistical framework for analyzing data obtained from this quantitative barcode sequencing of complex mixtures of mutants over time that accounts for the multiple sources of variation in these experiments.

Through application of this method we quantified the survival of individual mutants when starved for either phosphate or leucine over a 3-week period. Using the increased resolution of quantitative sequencing of barcodes and multiple sampling during the starvation period we were able to determine individual survival profiles in each condition for more than half the genes in the genome. Using an exponential death model estimated by Poisson generalized linear regression we determined the rate of death for each mutant in both conditions, allowing us to treat survival as a quantitative trait.

Through bioinformatic analysis of the genes affecting survival, we found that cell cycle exit, aging, and survival are multifactorial processes involving several molecular functions. We found that mitochondrial function is critical to survival of cells starved for phosphate and enhances the rapid loss of viability observed in leucine-starved cells, indicating that respirative metabolism is required for proper response to nutrient depletion even in the presence of excess glucose. Our method also identified genetic evidence for important roles of autophagy in the survival of cells starved for phosphate and leucine. We find evidence for several additional processes and functions including mRNA processing, chromatin remodeling, and cytoskeleton functions that

appear to be uniquely related to survival in phosphate starvation conditions.

Our experimental and analytical methods represent a general approach to quantitative multiplexed genetic screens that makes possible new types of genetic studies in which the aim is to identify those genetic modules that function in particular cellular processes and events. By treating heretofore-qualitative phenotypes as quantitative traits it may be possible to achieve a higher-resolution genotype–phenotype map and infer new relationships between genes and the processes that they govern.

MATERIALS AND METHODS

Strains: The *S. cerevisiae* haploid deletion collection (YSC1063, Open Biosystems, YKO *Matα his3Δ1 leu2Δ0 lys2Δ0 ura3Δ0*) was manually transferred as clonal isolates from 96-well glycerol stock plates to YPD agar plates + 200 μg/ml G418 and grown at 30° for 3 days. To construct the mixtures of all mutants, complete colonies were harvested by addition of 5 ml water to each plate and subsequently pooled. Glycerol was added to a final concentration of 15% and aliquots of 2 ml, containing 1.8×10^9 cells/ml, were frozen at −80°.

Media and growth conditions: Chemically defined media were based on Saldanha *et al.* (2004), with modifications to chemically complement auxotrophies present in the deletion collection strain. For both phosphate and leucine limiting media we used 5.0 g/liter $(NH_4)_2SO_4$, 0.50 g/liter $MgSO_4 \cdot 7H_2O$, 0.10 g/liter $CaCl_2 \cdot 2H_2O$, 0.10 g/liter NaCl, 40 mg/liter histidine, 40 mg/liter uracil, and 60 mg/liter lysine. For phosphate limiting media we added 200 mg/liter leucine and 1.0 g/liter KCl. The only source of phosphorus in phosphate limiting media was KH_2PO_4, which was present at an initial concentration of 5 mg/liter. For leucine limiting media we added 1.0 g/liter KH_2PO_4 and 20 mg/liter leucine. We made each medium both with and without 200 μg/mL G418. Phosphate and leucine concentrations are well within previously defined limiting ranges (Saldanha *et al.* 2004; Boer *et al.* 2008).

We inoculated 400 ml of medium with 1.6 ml (2.9×10^9 cells) of the pooled deletion collection pool in 500-ml vessels (Infors). The culture was grown at 30°, agitated at 400 rpm with an impeller, and aerated with 5 liters/min filtered and humidified air. The pH was constantly measured and maintained at 5.0 throughout by the automated addition of 0.1 m KOH. Samples of 1-ml volume were taken at 0, 24, 48, 72, 99, 144, 240, and 473 hr.

Determination of population parameters: Each sample was sonicated to disrupt adhesive cells. The number of cells per milliliter and the average cell volume were determined using a Beckman Coulter counter. The number of viable cells was determined by manually counting colony-forming units (CFUs) after plating a known number of cells on YPD-agar plates and incubating at 30° for 2 days. Each data point is an average of at least two replicates. Typically, 1000 colonies were counted per time point when viability permitted. Population viability was defined as the percentage of plated cells that formed a CFU.

Extraction of DNA from viable fraction of mutant populations: To enrich for viable cells we performed an overnight outgrowth of the starved population. We placed a 1-ml sample of the starved population in 50 ml of supplemented minimal medium [5.0 g/liter $(NH_4)_2SO_4$, 1.0 g/liter KH_2PO_4, 0.50 g/liter $MgSO_4 \cdot 7H_2O$, 0.10 g/liter $CaCl_2 \cdot 2H_2O$, 0.10 g/liter NaCl, 40 mg/liter histidine, 40 mg/liter uracil, 60 mg/liter lysine, 200 mg/liter leucine, trace metals and vitamins, and 2% glucose]. Cells were grown for 24 hr in supplemented minimal medium before being harvested for DNA isolation. Genomic DNA was extracted using the QIAGEN (Valencia, CA) Genomic Tip system.

PCR amplification for quantitative barcode sequencing: We amplified molecular barcodes from genomic DNA and incorporated adaptors for the Illumina Genome Analyzer in a single step using tailed PCR primers (Illumina Genome Analyzer adaptor sequences are underlined in italics). Uptags were amplified using the primers Illumina-uptag (5′-*AAT GAT ACG GCG ACC ACC GAG ATC T*GAT GTC CAC GAG GTC TCT-3′) and Illumina-UPKANMX (5′-*CAA GCA GAA GAC GGC ATA CGA* GTC GAC CTG CAG CGT ACG-3′). Downtags were amplified in a separate reaction with the primers Illumina-downtag (5′-*AAT GAT ACG GCG ACC ACC GAG ATC T* CGG TGT CGG TCT CGT AG-3′) and Illumina-DNKANMX (5′-*CAA GCA GAA GAC GGC ATA CGA* GAA AAC GAG CTC GAA TTC ATC G-3′). We amplified barcodes using a high-fidelity thermostable polymerase (TaKaRa PrimeSTAR) from 200 ng of genomic DNA in 20-μl reactions with each primer at a final concentration of 1 μm. PCR products were visualized on a 2% agarose gel to confirm the generation of an ∼110-bp PCR product. We purified PCR products from excess primer and PCR reagents using QIAGEN PCR cleanup columns. We quantified the total yield of purified PCR product using a fluorometer and diluted the ∼110-bp product to 10 nm concentration corresponding to a concentration of 0.68 ng/μl.

Quantitative barcode sequencing using an Illumina Genome Analyzer II: We combined the PCR products from the separately amplified uptag and downtag reactions from each sample in equimolar amounts and added them to the same lane of an Illumina Genome Analyzer flow cell, following the manufacturer's protocol. To simultaneously sequence the uptags and downtags in the same lane we added two custom sequencing primers in equimolar amounts that were complementary to either the uptag or the downtag sequence. The uptag-sequencing primer (5′-CGA CCA CC GAGA TCT GAT GTC CAC-3′) is complementary to the U1 sequence and the downtag-sequencing primer (5′-GAC CAC CGA GAT CTC GGT GTC GGT C-3′) is complementary to the D1 sequence of the deletion cassette. Both sequencing primers lie 3 bases from the start of the barcode sequence. This enables sequencing of a three-nucleotide sequence that identifies the barcode as either an uptag (sequence index TCT) or a downtag (sequence index TAG) before sequencing the unique 20-base barcode sequence.

Barcodes were sequenced using 36-base sequencing cycles. Sequencing data were processed using the Illumina pipeline (Gerald, Bustard). FASTQ files for each sequencing run were processed with custom Perl scripts to determine the identity and number of each barcode. A complete list of sequencing experiments and number of mapped barcode reads is provided (supporting information, Table S1).

Normalization of barcode counts: We determined the total number of uptags and downtags sequenced in each lane using the unique 3-base prefix. We then determined the total number of counts for each unique known barcode. We tested only for exact matches to known barcodes and did not consider individual base quality metrics. For each sequence run, ∼25% of barcodes could not be exactly mapped to a known barcode. Therefore, the presence of the 3-base index was essential for accurate normalization of uptag and downtag counts. For initial comparisons and cluster analyses we converted barcode counts to a frequency by dividing the abundance of each unique barcode by the total number of uptags or downtags.

For modeling the death rates of strains over the time course, we normalized the data within each starvation experiment to

preserve the scale of the original barcode counts. Briefly, let $x_i(t_j)$ be the number of reads for barcode i at time point t_j, ($t_1 = 24$, $t_2 = 48$, . . . , $t_7 = 473$) and let N_j be the total number of reads corresponding to sequencing lane j. We formed weights $w_j = 7 \times N_j / \sum_{k=1}^{7} N_k$ and calculated normalized counts by $y_i(t_j) = w_j \times x_i(t_j)$ for each barcode i and lane j.

Cluster analysis: We performed hierarchical cluster analysis using Cluster 3 (De Hoon *et al.* 2004). For clustering we computed the Euclidean distance between $\log_2$-tranformed proportional data for each time point that had been normalized to the initial time point ($t = 24$ hr) using complete linkage. Clustering was visualized using JavaTreeView (Saldanha 2004). Gene ontology (GO) term enrichment analysis was performed using GoTermFinder (Boyle *et al.* 2004).

Model fitting and inference: All model fitting and inference were performed using the statistical software package R. As described above, let $y_i(t_j)$ be the normalized number of sequencing reads for barcode i at time point t_j. We initially modeled $y_i(t_j) \sim \text{Poisson}(\exp[a_i - b_i t_j])$, where b_i quantifies the *relative* (to the total population) death rate per hour for the strain corresponding to barcode i, and $h_i = \ln(2)/b_i$ represents the *relative* half-life. We performed a Poisson generalized linear regression to estimate a_i and b_i. An inspection of the deviances revealed that there is a systematic overdispersion, meaning the variance is larger than expected under the Poisson model. This makes sense because there are several levels of variation experimentally induced beyond the assumed exponential death rate. Therefore, we fit the above model using an overdispersed Poisson error model (via the R function glm with family = quasipoisson).

The counts for each barcode at a specific time point measure the abundance of the corresponding strain relative to the entire population. Therefore, a "flat" pattern across time points ($b_i = 0$) according to the above model indicates the strain corresponding to that barcode dies at a rate equal to the overall population death rate.

To quantify the absolute death rates, we took into account the percentage of the population alive at each time point (see *Determination of population parameters* above). Let p_1, p_2, . . . , p_7 be the percentages corresponding to the seven time points at which sampling occurred. We calculated weights $v_j = 7 \times p_j / \sum_{k=1}^{7} p_k$ to form counts $z_i(t_j) = v_j \times y_i(t_j)$ that capture the absolute change in strain abundance over time. We modeled the $z_i(t_j)$ according to an overdispersed Poisson generalized linear regression as before to obtain estimates of the absolute death rates and half-lives. In this case a flat pattern across time points ($b_i = 0$) indicates that the strain has no death across the time points.

All inference (hypothesis testing and confidence intervals) on the death rates b_i and half-lives $h_i = \ln(2)/b_i$ was performed using the default settings from the glm function under the overdispersed Poisson model (family = quasipoisson) in R. Specifically, p-values were obtained for each barcode i in testing $b_i = 0$ for both the relative and the absolute analyses, and false discovery rate (FDR) q-values were obtained to form significance thresholds (Storey and Tibshirani 2003).

Gene function enrichment analysis: We performed gene class function enrichment analysis by comparing the distribution of half-lives for defined subsets of genes to the distribution of all half-lives in which the values for the query set had been removed. We assessed the statistical significance of the difference between these two distributions using a Wilcoxon–Mann–Whitney test in R. Gene sets were defined by GO terms from all three ontologies (process, function, and location) and GO Slim terms, biochemical pathways, and protein complexes as defined using annotated data available through the Saccharomyces Genome Database (SGD) (http://downloads.yeastgenome.org/literature_curation/) accessed on March 9th 2010. In addition, we used high-throughput studies of the yeast deletion collection and a subset of genome-wide transcript profiling studies to define phenotypic classes. We applied a p-value cutoff of 0.001 for identifying gene classes exhibiting nonrandom distributions of half-lives. Given that we tested 528 gene classes, this implies we expect 0.5 false positives among the results that pass this significance threshold.

RESULTS

The first nutrient depleted determines the rate of population death: To investigate the survival of all viable haploid (*MAT*α) deletion mutants to defined starvation states we inoculated cultures with mixtures containing the entire mutant library. To ensure precise control of the starvation conditions we used media that are similar to the commonly used yeast minimal media, but composed entirely of chemically defined components (materials and methods). In these media all components are in excess and one nutrient is present at limiting concentration; *i.e.*, it is the first nutrient that is exhausted in the culture. Allowing cells to deplete the limiting nutrient rather than switching cells to medium lacking a particular nutrient allows cells to adjust to decreasing amounts of the limiting nutrient. This is likely to be important as previous studies suggest that starvation responses are initiated well before nutrients are depleted and cell cycle exit occurs (Lillie and Pringle 1980). The genotype of all deletion mutants contains four auxotrophic alleles: *his3*Δ*1*, *leu2*Δ*0*, *lys2*Δ*0*, and *ura3*Δ*0*. To compare survival of mutants in response to a natural and an unnatural limitation we used media in which either phosphate or leucine is the first nutrient exhausted (Saldanha *et al.* 2004; Boer *et al.* 2008).

We inoculated four independent cultures with 2.9×10^9 cells each. Thus, each of the ~4800 viable deletions was initially represented by $\sim 6 \times 10^5$ clonal individuals in the inoculums. Each of the two nutrient limiting conditions was imposed in two separate cultures that differed only by the presence of the antibiotic, kanamycin, to aid in maintaining culture sterility. Following 24 hr of culture growth we measured survival of mutants in each starvation condition by determining population viability at multiple time points. We observed a dramatic and reproducible difference in survival profiles that distinguishes populations starved for leucine from those starved for phosphate (Figure 1A). In the case of phosphate starvation, the viability of the heterogeneous mutant pool remains high throughout the starvation period and ~30% of the population is viable following nearly 500 hr of starvation. In contrast, populations starved for leucine survive poorly and <1% of the population is viable after starvation for leucine over the same time period. We quantified population survival according to an exponential death rate and applied a Poisson generalized linear model to

the viability data in each experiment. We determined that the mixed population of null mutants starved for phosphate dies at a rate of 0.20%/hr (population half-life = 337 hr) whereas the same population of mutants starved for leucine dies at a rate of 2.5%/hr (population half-life = 27.7 hr). This order of magnitude difference in loss of viability is consistent with our previous results using individual strains (Boer *et al.* 2008) and demonstrates that the fate of starved cells depends on which nutrient is exhausted in the population first.

Population sizes of $\sim 1.5 \times 10^{10}$ and 1.3×10^{10} in the phosphate- and leucine-starved conditions, respectively, remained essentially constant in replicate populations throughout the starvation periods (Figure 1B). The turbidity of phosphate-starved populations appeared to increase gradually during the starvation period whereas the leucine-starved population appeared to decrease (Figure 1C). This may be related to the fact that average cell volume increased in phosphate-starved populations but decreased in leucine-starved populations (Figure 1D). We observed a similar trend in cultures grown under continuous phosphate or leucine limitation in chemostats (Brauer *et al.* 2008) and this size difference may reflect differences in the volume of vacuoles associated with starvation.

Quantitative barcode sequencing: The central challenge in performing multiplex screens of mutant populations is accurate determination of the abundance of each individual mutant. When the yeast gene deletion collection was constructed, unique molecular sequences of 20 nucleotides were included on either side of the kanamycin resistance marker used to replace each open reading frame (Giaever *et al.* 2002). These molecular barcodes, which can be PCR amplified using common priming sites, enable the identification of each mutant by assaying for the presence or absence of each unique barcode. Typically, mutant identification in pooled experiments has been achieved by hybridization of the PCR products to DNA microarrays containing sequences complementary to each barcode (Giaever *et al.* 2002). Measurement of the relative abundance of each barcode makes it possible to infer the frequencies of each mutant in a complex mixture of genotypes.

We reasoned that quantitative sequencing of molecular barcodes using new high-throughput sequencing methods would provide increased accuracy and dynamic range. Therefore, we developed a method of quantitative barcode sequencing to estimate the frequency of each mutant in heterogeneous populations. This method is designed for use with the Illumina Genome Analyzer II and is similar to a recently reported method (Smith *et al.* 2009). In addition, we developed new methods for analyzing data generated using this approach (see materials and methods).

We undertook a series of control experiments to validate the utility of quantitative sequencing as a means

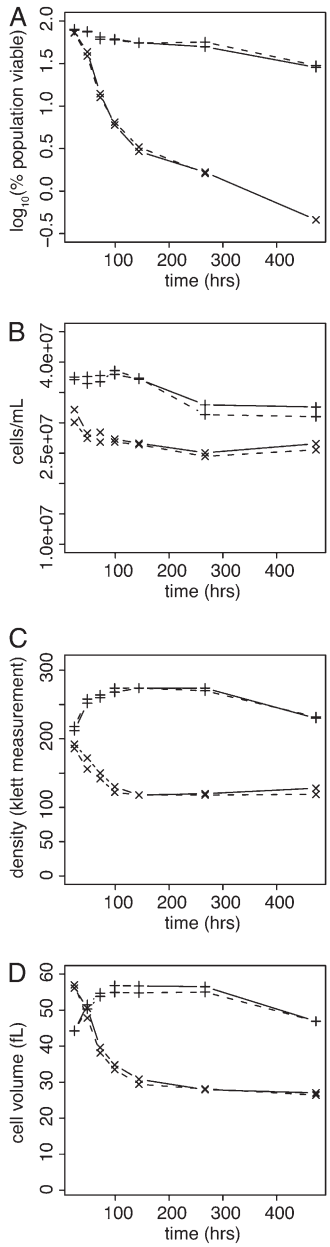

Figure 1.—Survival and physiological parameters for heterogeneous mutant populations during starvation conditions. The entire collection of haploid deletion mutants was starved for either phosphate (+) or leucine (x) in the presence (solid line) or absence (dashed line) of kanamycin for nearly 500 hr following an initial period of 24 hr of batch growth. (A) Survival of replicate populations grown in media of identical composition except for the limiting nutrient. Survival of each population was monitored by determining viability of the population at each time point by counting CFUs on rich media plates. (B) The total number of cells per milliliter was determined at each time point and remained essentially unchanged throughout the starvation regime. (C) Culture biomass was estimated using a Klett colorimeter and showed a gradual increase for populations starved for phosphate and gradual decrease when populations were starved for leucine. (D) The average cell volume, measured using a Coulter counter, showed a gradual increase for populations starved for phosphate and a slow decline for populations starved for leucine.

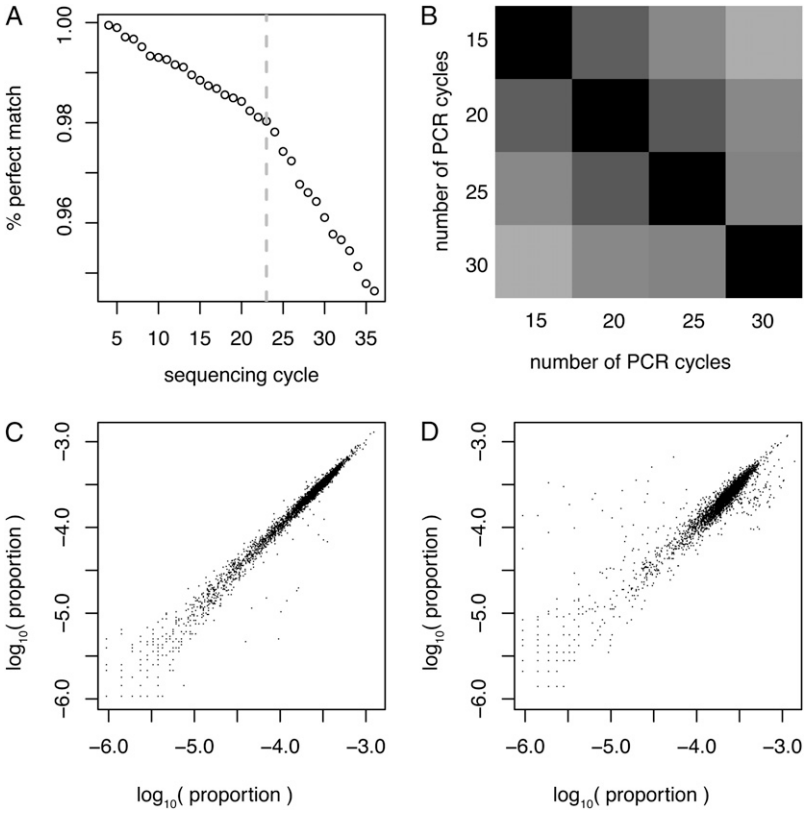

FIGURE 2.—Development and validation of quantitative barcode sequencing for multiplexed mutant screens. We tested the error and variance associated with each step of our protocol. (A) By sequencing a single barcode we found that 98% of sequences up to sequencing cycle 23 (dashed line) perfectly match the expected sequence ($n = 2{,}340{,}984$). (B) Additional cycles of PCR introduce minimal variation in the estimated proportions of mutants. The best-correlated estimates of mutant abundance are found between 15 and 25 PCR cycles (increasingly darker shaded values approach a correlation of 1.0; the minimum correlation is 0.94). (C) Resequencing the same PCR product from a complex mixture of mutants on two different flow cells yields highly reproducible results (Pearson's correlation = 0.99; $n = 3329$). (D) Complete technical replicates of quantitative barcode sequencing (*i.e.*, independent DNA preparations, PCR, and sequencing reactions) are highly reproducible (Pearson's correlation = 0.94; $n = 3439$).

of determining barcode frequencies in mixed populations. First, to determine the false negative rate due to sequencing error, we sequenced a single barcode. We obtained 2,340,984 sequences that passed sequence analysis filters (see Table S1 for a complete summary of sequencing results for this study) and for each sequencing cycle we determined the fraction of reads that perfectly matched those bases in the known barcode sequence. We identified a decline in sequencing accuracy with each additional sequencing cycle (Figure 2A). As the molecular barcodes are only 20 bases in length and our sequencing primers lie 3 bases from the beginning of each barcode, we are concerned only with the first 23 sequenced bases in this study. Therefore, we estimate the fraction of incorrectly sequenced barcodes to be <2% in each experiment.

To test the sources of variation and the reproducibility of quantitative sequencing of barcodes we investigated the effect of each step in our protocol. Recovery of barcode sequences from genomic DNA requires an initial PCR amplification of the barcodes. As PCR is an exponential process, it is conceivable that noise will increase with the number of PCR cycles. Therefore, we investigated the effect of additional PCR cycles on barcode counts by sequencing aliquots removed from a single PCR reaction tube after 15, 20, 25, and 30 cycles of amplification (Figure 2B). We found good correlation between the estimated relative abundance of each barcode following each additional five rounds of PCR. The poorest correlation is between 30 cycles and all previous cycles, which may be a result of PCR reagents becoming limiting after 25 cycles as we found that the total yield (in mass) of DNA from the reaction reached a plateau at 25 cycles (data not shown). We conclude that PCR amplification of barcodes is linear up to 25 cycles under these conditions and the optimal number of cycles, which provides both sufficient yield and linearity of amplification, is 20 PCR cycles.

We found extremely high reproducibility of normalized barcode counts when the same PCR reaction from a complex pool of mutants was sequenced on two different flow cells (Figure 2C). Finally, we performed replicate DNA preparations, PCR, and sequencing reactions of the same heterogeneous sample and confirmed that results are extremely well correlated (Figure 2D). As we routinely obtained $>6 \times 10^6$ individual sequences per sample, there are theoretically over six orders of magnitude of dynamic range available. We sequenced uptags and downtags from each biological sample in the same lane within a flow cell and for the purposes of analyses we treated uptag and downtag measurements as individual measures of mutant abundance. For each sequencing reaction ~25% of reads did not perfectly match a known barcode (Table S1). Since we estimated our sequencing error to be <2%, we assumed that unidentified barcodes were primarily due to errors in the strains' barcodes as opposed to sequence errors. These data were excluded from further analyses.

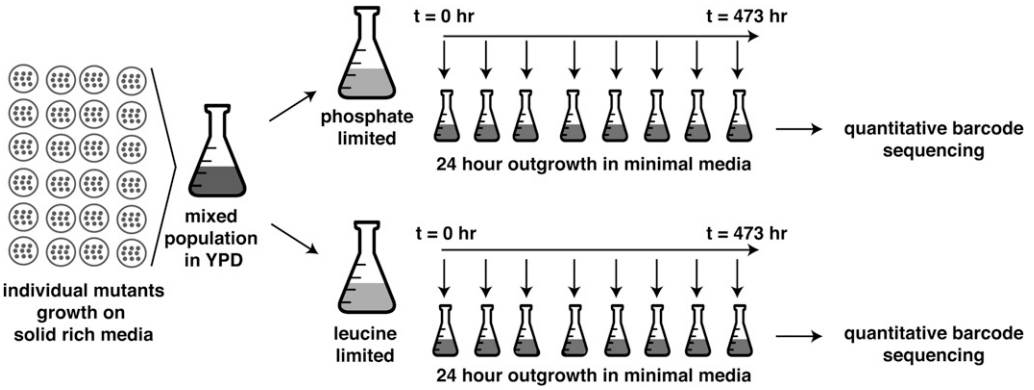

FIGURE 3.—Experimental design for multiplexed mutant survival analysis using quantitative barcode sequencing. We constructed normalized pools of the yeast haploid deletion collection by growing individual mutants on rich media (YDP) plates and pooling mutants in liquid YPD for archival purposes. A 1.6-ml aliquot of the unselected pooled mutants was used to inoculate ($t = 0$) cultures limited for either phosphate or leucine. The starvation period commenced after 24 hr of culture growth. At each time point we removed a 1-ml sample from the culture and expanded the viable subpopulation by allowing 24 hr of outgrowth in supplemented minimal media. DNA was isolated from the resulting culture and analyzed using quantitative barcode sequencing.

Experimental design for multiplexed survival analysis: We developed an experimental design that allowed multiplex analysis of individual mutant survival upon defined starvation using quantitative barcode sequencing (Figure 3 and MATERIALS AND METHODS). Mixtures of mutant strains were constructed by growing individual mutants on solid rich media and subsequently pooling them. An aliquot of the heterogeneous population was used to inoculate cultures limited for either phosphate or leucine. Population growth ceased 24 hr after inoculation and we define this point as initiation of the starvation phase. At each time point we removed a sample from the population and performed a 24-hr outgrowth in supplemented minimal medium. This step was required to enrich mutants that survive starvation from those that have perished. By performing the identical outgrowth step at every time point, and determining the rate of change in strain abundance in the viable fraction of the population, our design normalizes for any growth rate differences between mutants during the outgrowth.

We used our quantitative sequencing method to determine the change in population composition prior to initiation of starvation. Sequence analysis of the unselected pooled samples identified 7016 unique barcodes corresponding to 4497 unique strains. Therefore, sequencing of both uptag and downtag barcodes for each strain results in almost complete (93.5%) identification of the expected nonessential haploid gene deletion strains. We compared mutants detected in unselected pooled samples with our initial inocula ($t = 0$) in both nutrient-limited cultures. As we performed outgrowth in supplemented minimal media for each time point in our experiment (MATERIALS AND METHODS), including the $t = 0$ point, this analysis identifies those mutants that are able to grow in rich laboratory media but unable to grow in supplemented minimal medium. We identified 73 mutant strains that were well measured in the unselected pool but reduced in abundance by >100-fold in the $t = 0$ sample in both the leucine and the phosphate starvation experiments (Table 1). Consistent with our expectation, mutants that are unable to survive the outgrowth in supplemented minimal media are strongly enriched for the GO process term "cellular nitrogen compound biosynthetic process" (42 of 74 genes; genome frequency = 4.5%; $P = 1.7 \times 10^{-35}$) and include many of the known auxotrophies that are unable to grow in the absence of nutritional supplementation. In addition, strains mutant for regulation of biosynthetic pathways (*GCN3* and *GCN4*), RAS signaling (*SRV2*), iron–sulfur cluster biogenesis (*ISA1* and *ISA2*), and protein and phosphatidylinositol kinase activity important for vacuolar targeting of proteins (*VPS15* and *VPS34*) were purged from the population during this initial outgrowth. Our ability to specifically identify this expected class of mutants in our heterogeneous pool of mutants provided additional validation of the utility of our quantitative barcode sequencing method.

Survival trends during prolonged nutrient starvation: We analyzed changes in the diversity of phosphate- and leucine-starved populations at each time point during the starvation experiments, using quantitative barcode sequencing. First, we counted the number of unique strains detected at each time point (Figure 4A). Most strains persist in the population at some level for the first 144 hr following inoculation in both media. The greatest distinction in population diversity was observed at the final two time points. At $t = 267$ hr, 78% (3165 of 4033) of strains initially present in the population remained detectable in the leucine starvation condition whereas 96% (3948 of 4087) of strains initially present in the phosphate-starved population were detected. This difference was more pronounced after 473 hr at which point only 37% of the initial strains were detected in the leucine-starved population (1169 of 4033) and 86% (3528 of 4087) of strains were detected in the phosphate-starved population. On average, 1 strain is

TABLE 1

Mutants purged from the population due to outgrowth in supplemented minimal media

Mutants
AAT2, *ACO1*, *ADE1*, *ADE12*, *ADE2*, *ADE3*, *ADE4*, *ADE5,7*, *ADE6*, *ADE8*, *ARG1*, *ARG2*, *ARG3*, *ARG4*, *ARG5,6*, *ARO2*, *ARO7*, *ATE1*, *BRO1*, *BUD25*, *BUD32*, *CAF17*, *CDC40*, *CPA1*, *CPA2*, *CYS4*, *DOC1*, *ECM29*, *GCN3*, *GCN4*, *GND1*, *GON7*, *GRX5*, *HFI1*, *HOM3*, *HOM6*, *ILV1*, *ISA1*, *ISA2*, *MET6*, *MET7*, *MOT2*, *ORT1*, *PEP7*, *PHA2*, *POS5*, *RIB4*, *RNR1*, *RPL27A*, *SER1*, *SER2*, *SHM2*, *SLA2*, *SPT7*, *SRV2*, *STB5*, *THR1*, *THR4*, *TRP1*, *TRP2*, *TRP3*, *TRP4*, *TRP5*, *TYR1*, *VPS15*, *VPS34*, *YDR008C*, *YER068C-A*,[a] *YER091C-A*, *YIL039W*, *YKR041W*, *YOR302W*,[b] *YOR364W*, *ZWF1*

We compared the mutants detected in mixed populations constructed by growth on rich media with mutants in the leucine- and phosphate-limited cultures immediately following inoculation ($t = 0$ hr) and outgrowth for 24 hr in supplemented minimal media.

Mutants primarily include auxotrophic strains that were not chemically complemented during the outgrowth.

[a] *YER068C-A* is a dubious ORF encoded on the strand opposite *ARG5,6*.

[b] *YOR302W* is an upstream ORF that regulates translation of *CPA1*.

lost from the population per hour of phosphate starvation but 6 strains are lost from the population per hour of leucine starvation. These observations are consistent with starvation of a leucine auxotroph for leucine imposing a much stronger selection on cells than starvation for phosphate.

We performed hierarchical clustering of relative changes in individual mutant abundance during both starvation regimes (Figure 4B). For this purpose, the relative abundance of each mutant was determined in the population and expressed as the ratio of abundance at each time point to the abundance of that mutant at the commencement of starvation ($t = 24$ hr; values are $\log_2$ transformed). Thus, this analysis distinguishes those mutants that increase in representation in the population from those that decrease in representation. In the clustered data we frequently observe the uptag and downtag (separately PCR amplified) coclustering. Two general trends are apparent in the resulting clustergram. First, most deletion mutants are unchanged in relative abundance throughout phosphate starvation but change in relative abundance to a far greater degree during leucine starvation. Second, in both starvation regimes the majority of deletion mutants are reduced in relative abundance. This indicates that the typical effect of a deletion mutation on survival is detrimental and a minority of mutants are able to increase in relative abundance through increased relative survival.

We identified a number of interesting clusters that distinguish mutant survival profiles in the two different conditions and provide qualitative evidence consistent with our expectations. A cluster of mutants appears to be specifically reduced in relative abundance upon starvation for phosphate (Figure 4C). This cluster includes null mutants of *PHO4*, a transcriptional regulator of the phosphate starvation response, *PHO81*, the cyclin-dependent kinase inhibitor required for inhibition of the *PHO80–PHO85* cyclin-dependent kinase upon phosphate starvation, and *PHO84*, which encodes a high-affinity inorganic phosphate transporter. We identified a cluster including several mutants that increase in relative abundance when starved for leucine but not phosphate (Figure 4D). This cluster includes the mutants *TOR1*Δ0 and *PPM1*Δ*0*, which we previously recovered as spontaneous loss-of-function mutants in a genetic screen for increased survival upon leucine starvation (Boer *et al.* 2008). Loss of *TOR1* signaling has been reported to promote longevity in yeast (Powers *et al.* 2006; Wei *et al.* 2008). Significantly, our analysis shows that the *TOR1*Δ*0* strain is not altered in relative abundance in the phosphate-starved population suggesting that its loss of function does not confer increased survival in phosphate starvation conditions. A cluster of null mutants that decline in relative abundance when starved for either phosphate or leucine (Figure 4E) contains several strains mutant for autophagy genes (*ATG1*, *ATG2*, *ATG3*, *ATG7*, *ATG9*, *ATG12*, *ATG15*, *ATG17*, *ATG18*, and *ATG21*). Autophagy, the process by which cells degrade cellular components, is an important process for survival of nutrient starvation (Takeshige *et al.* 1992). It is noteworthy that we failed to identify a cluster of mutants that *increase* in relative abundance in both phosphate and leucine starvation.

Quantitation of relative change in individual abundance: We tested each strain for significant change in relative abundance (compared to the total population) throughout the starvation periods (materials and methods). We determined that 1333 of 4337 strains (32%) starved for phosphate differed significantly in their relative abundance during the experiment (Table S2). By contrast 3951 of 4299 mutant strains (92%) starved for leucine were significantly altered in their relative abundance (Table S3). The majority of leucine-starved null mutants were significantly decreased in relative abundance (3500 mutants; 88.6%), but 458 (11.6%) mutants increased in relative abundance. For mutants starved for phosphate, 956 (71.7%) were significantly decreased in relative abundance and 377 (28.3%) increased in relative abundance.

The majority of null alleles that increased in relative abundance in either leucine or phosphate starvation are nonoverlapping. By contrast, an overlapping set of 785 null mutants was significantly decreased in relative abundance when starved for either phosphate or leucine. We performed GO term enrichment analysis of mutants that are increased or decreased in relative abundance, regardless of the magnitude of the change, in either condition or both (Table 2 and materials and

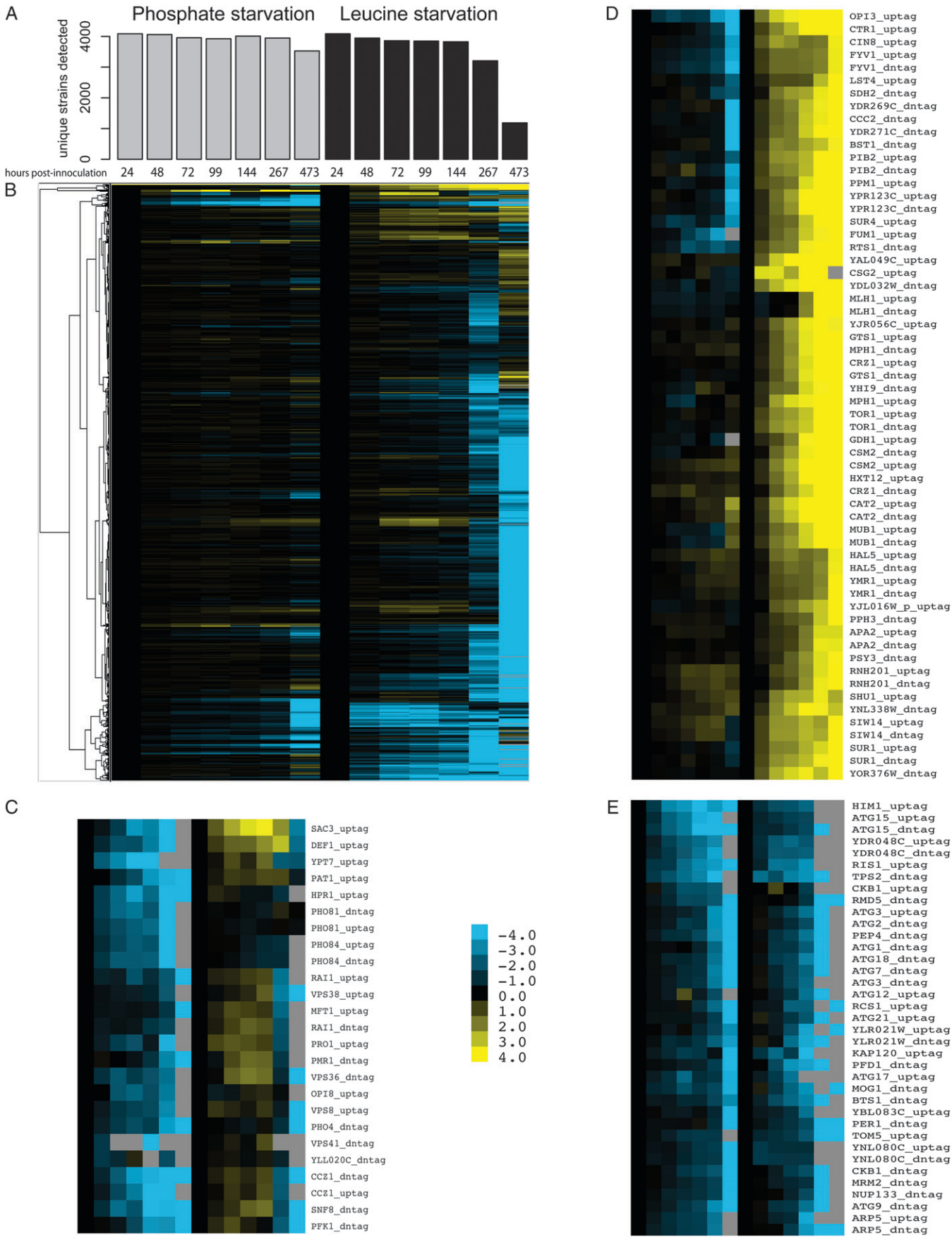
A
Phosphate starvation
Leucine starvation
unique strains detected
0
2000
4000
hours post-innoculation
24 48 72 99 144 267 473 24 48 72 99 144 267 473
B
C
SAC3_uptag
DEF1_uptag
YPT7_uptag
PAT1_uptag
HPR1_uptag
PHO81_dntag
PHO81_uptag
PHO84_uptag
PHO84_dntag
RAI1_uptag
VPS38_uptag
MFT1_uptag
RAI1_dntag
PRO1_uptag
PMR1_dntag
VPS36_dntag
OPI8_uptag
VPS8_uptag
PHO4_dntag
VPS41_dntag
YLL020C_dntag
CCZ1_dntag
CCZ1_uptag
SNF8_dntag
PFK1_dntag
-4.0
-3.0
-2.0
-1.0
0.0
1.0
2.0
3.0
4.0
D
OPI3_uptag
CTR1_uptag
CIN8_uptag
FYV1_uptag
FYV1_dntag
LST4_uptag
SDH2_dntag
YDR269C_dntag
CCC2_dntag
YDR271C_dntag
BST1_dntag
PIB2_uptag
PIB2_dntag
PPM1_uptag
YPR123C_uptag
YPR123C_dntag
SUR4_uptag
FUM1_uptag
RTS1_dntag
YAL049C_uptag
CSG2_uptag
YDL032W_dntag
MLH1_uptag
MLH1_dntag
YJR056C_uptag
GTS1_uptag
MPH1_dntag
CRZ1_uptag
GTS1_dntag
YHI9_dntag
MPH1_uptag
TOR1_uptag
TOR1_dntag
GDH1_uptag
CSM2_dntag
CSM2_uptag
HXT12_uptag
CRZ1_dntag
CAT2_uptag
CAT2_dntag
MUB1_uptag
MUB1_dntag
HAL5_uptag
HAL5_dntag
YMR1_uptag
YMR1_dntag
YJL016W_p_uptag
PPH3_dntag
APA2_uptag
APA2_dntag
PSY3_dntag
RNH201_uptag
RNH201_dntag
SHU1_uptag
YNL338W_dntag
SIW14_uptag
SIW14_dntag
SUR1_uptag
SUR1_dntag
YOR376W_dntag
E
HIM1_uptag
ATG15_uptag
ATG15_dntag
YDR048C_uptag
YDR048C_dntag
RIS1_uptag
TPS2_dntag
CKB1_uptag
RMD5_dntag
ATG3_uptag
ATG2_dntag
PEP4_dntag
ATG1_dntag
ATG18_dntag
ATG7_dntag
ATG3_dntag
ATG12_uptag
RCS1_uptag
ATG21_uptag
YLR021W_uptag
YLR021W_dntag
KAP120_uptag
PFD1_dntag
ATG17_uptag
MOG1_dntag
BTS1_dntag
YBL083C_uptag
PER1_dntag
TOM5_uptag
YNL080C_uptag
YNL080C_dntag
CKB1_dntag
MRM2_dntag
NUP133_dntag
ATG9_dntag
ARP5_uptag
ARP5_dntag

METHODS). We found significant enrichment for several GO terms for genes that are reduced in relative abundance in starvation conditions that are related to both autophagy (both nuclear and mitochondrial) and vacuolar transport. In addition, several GO terms unique to mutants reduced in relative abundance during phosphate starvation are related to mitochondrial function and chromatin. We found few GO terms associated with mutants that are increased in relative survival. Uniquely in leucine starvation conditions we find mutants annotated to transcription factor activity and peroxisomal transport increase in relative abundance.

Quantitation of absolute rates of mutant death: Ideally, multiplexed analysis of mutants generates equivalent data to those obtained by testing each mutant individually. For our purposes, experiments performed on individual mutants determine the absolute rate of cell death. We sought to extract this rate from our multiplexed data by estimating the absolute number of each genotype using relative strain abundance and total population viability simultaneously (MATERIALS AND METHODS). To test the accuracy of our method of absolute rate estimation we determined the rate of death of a neutral deletion strain, the deletion of the *HO* locus, in the mixed population with estimates of the death rate determined for the isogenic strain BY4742 determined in an individual assay. We estimate a death rate for the HO knockout strain in the phosphate starvation regime of 0.22%/hr on the basis of both the uptag and the downtag (Figure 5A). The identical death rate is found when BY4742 is starved for phosphate as a pure culture (Figure 5A). When starved for leucine, BY4742 dies at a rate of 2.2%, which is not statistically different from the estimated death rate of the HO knockout strain in the leucine-starved population, which we estimate to be 2.88%/hr (uptag value) and 2.77%/hr (downtag value) (Figure 5B). This demonstrates that our combined experimental and analytical methods allow us to obtain absolute rates of death from the pooled experiment that are good estimates of rates obtained by performing starvation experiments for each strain individually.

We fit an overdispersed Poisson generalized regression model to estimated absolute mutant abundance data for 6806 unique barcodes corresponding to 4337 unique strains in the phosphate starvation experiment and 6730 unique barcodes corresponding to 4293 unique strains in the leucine starvation experiment. On the basis of this analysis we determined significant death rate estimates (FDR $< 5\%$) for 4143 strains starved for phosphate (Table S4) and 3591 strains starved for leucine (Table S5). We found good concordance between our results from the pooled experiments and individual mutant analysis for a small number of individually tested genotypes in both conditions (Figure S1).

We used the calculated death rates for each mutant to determine the distribution of half-lives for mutants starved for phosphate (Figure 5C) or leucine (Figure 5D), assuming an exponential death rate. The median half-life in each of these distributions is 288.6 hr for mutants starved for phosphate and 22.8 hr for mutants starved for leucine. The distributions are widely dispersed, consistent with many hundreds of genes altering survival in the two nutrient starvations.

Identification of nonrandomly distributed mutant classes: We hypothesized that functionally related mutants important for cell cycle exit, aging, and survival would exhibit similar half-lives when starved for either leucine or phosphate. Therefore, we compared the distribution of half-lives for *a priori* defined gene sets with the complete distribution of half-lives for each starvation, using the nonparametric Mann–Whitney–Wilcoxon test.

First, we tested gene sets defined by the complete GO annotation for yeast for nonrandom survival. Gene sets were also defined by the GO Slim categorization, which provides a less granulated classification of genes. We found that genes annotated to the GO Slim term "mitochondrial organization" are significantly reduced in survival when starved for phosphate (Figure 6A) and leucine (Figure 6B). Mutants annotated to several additional terms related to mitochondrial function have reduced survival in both experiments, including mitochondrial inner matrix (GO:0005743), cellular ATP synthesis coupled to proton transport (GO:0015986), and cytochrome-c oxidase activity (GO:0004129) (Table S6). We then tested gene sets defined by protein complex membership and identified significant results for mitochondrion and mitochondrial ribosome complexes (Table S6). Finally, we tested gene sets defined by global phenotypic analyses (GIAEVER *et al.* 2002; DUDLEY *et al.* 2005). Consistent with a role for mitochondrial function in survival in prolonged starvation states, we find that cells defective for growth on non-

FIGURE 4.—Population diversity decline and mutant abundance profiles during prolonged starvation. (A) We determined the number of unique strains identified through barcode sequencing at each time point for populations starved for phosphate (gray bars) or leucine (black bars). (B) Hierarchical clustering of mutant abundance profiles during starvation experiments. We clustered vectors of relative abundance in the population normalized by the abundance of each mutant at $t = 24$ hr ($\log_2$ transformed). Black indicates that the strain has not changed in abundance. Yellow represents increases in abundance and blue represents decreases in abundance. Failure to detect the strain in the population is indicated by gray. We identified clusters of mutants that were specifically either (C) decreased in relative abundance upon phosphate starvation or (D) increased in relative abundance upon leucine starvation. Several mutants are decreased in relative abundance under both starvation conditions including (E) a cluster including several autophagy gene mutants.

TABLE 2

GO term enrichment analysis of mutants that are significantly altered in relative abundance during starvation

Starvation condition	Relative abundance	GO term	*p*-value
Phosphate	Increased	None	
	Decreased	Process ontology	
		Vacuolar transport	1.87×10^{-13}
		Piecemeal microautophagy of nucleus	1.60×10^{-11}
		Microautophagy	1.21×10^{-9}
		Autophagy	3.13×10^{-9}
		Protein targeting to vacuole	3.21×10^{-9}
		Cellular catabolic process	1.88×10^{-8}
		Organelle organization	3.75×10^{-7}
		CVT pathway	4.74×10^{-7}
		Catabolic process	6.31×10^{-7}
		Mitochondrion degradation	6.37×10^{-6}
		Mitochondrion organization	1.92×10^{-5}
		Cellular macromolecule localization	2.89×10^{-5}
		Protein targeting	6.19×10^{-5}
		Establishment of localization in cell	8.60×10^{-5}
		Cellular protein localization	0.000106271
		Mitochondrial respiratory chain complex assembly	0.000145155
		Intracellular protein transport	0.000145634
		Cellular localization	0.000146596
		Cellular component organization	0.000220552
		Intracellular transport	0.000226577
		Chromatin modification	0.000333457
		Chromatin organization	0.000631496
		Macroautophagy	0.001464925
		Protein transport	0.002018461
		Macromolecule localization	0.00253975
		Establishment of protein localization	0.002878238
		Late endosome to vacuole transport	0.003306452
		Macromolecule catabolic process	0.003396641
		Cellular macromolecule catabolic process	0.004833406
		Component ontology	
		Mitochondrion	9.67×10^{-11}
		Mitochondrial part	4.11×10^{-9}
		Organelle membrane	1.37×10^{-7}
		Mitochondrial envelope	2.58×10^{-7}
		Organelle	2.73×10^{-7}
		Intracellular organelle	2.73×10^{-7}
		Membrane-bounded organelle	7.90×10^{-7}
		Intracellular membrane-bounded organelle	7.90×10^{-7}
		Cytoplasm	1.81×10^{-6}
		Membrane	1.82×10^{-6}
		Intracellular	1.86×10^{-6}
		Cytoplasmic part	2.50×10^{-6}
		Mitochondrial membrane	2.57×10^{-6}
		Intracellular part	6.41×10^{-6}
		Endosome	8.09×10^{-6}
		Cell part	1.04×10^{-5}
		Cell	1.11×10^{-5}
		Organelle envelope	1.16×10^{-5}
		Envelope	1.16×10^{-5}
		Mitochondrial inner membrane	1.73×10^{-5}
		Organelle inner membrane	1.86×10^{-5}
		Protein complex	3.14×10^{-5}
		Preautophagosomal structure	8.94×10^{-5}
		Endosomal part	0.00010005
		Endosome membrane	0.000482025
		Mitochondrial membrane part	0.0006434

(*continued*)

TABLE 2

(Continued)

Starvation condition	Relative abundance	GO term	*p*-value
		Membrane part	0.000749224
		Organelle part	0.00177721
		Intracellular organelle part	0.00177721
		Late endosome	0.005090903
		Late endosome membrane	0.007179905
Leucine	Increased	Function ontology	
		Transcription factor activity	0.005178439
		Process ontology	
		Peroxisomal transport	0.003125654
	Decreased	Function ontology	
		Transmembrane transporter activity	2.23×10^{-7}
		Phosphoric ester hydrolase activity	0.006618899
		Process ontology	
		Catabolic process	1.57×10^{-7}
		Response to stimulus	7.18×10^{-7}
		Response to chemical stimulus	1.40×10^{-6}
		Cellular catabolic process	6.39×10^{-6}
		Organic acid transport	2.75×10^{-5}
		Carboxylic acid transport	2.83×10^{-5}
		Vacuolar protein catabolic process	7.17×10^{-5}
		Reproductive cellular process	0.000117342
		Transport	0.000118658
		Ion transport	0.000149536
		Establishment of localization	0.000152932
		Filamentous growth	0.000206233
		Localization	0.000206468
		Cell differentiation	0.000211337
		Reproductive process in single-celled organism	0.000466565
		Amine transport	0.001303683
		Cellular response to chemical stimulus	0.002486978
		Biological regulation	0.002673032
		Sporulation resulting in formation of a cellular spore	0.004605798
		Sporulation	0.004605798
		Sexual reproduction	0.005551172
		Autophagy	0.0077015
		Transmembrane transport	0.008679718
		Component ontology	
		Intrinsic to membrane	2.36×10^{-18}
		Integral to membrane	2.18×10^{-16}
		Membrane part	5.20×10^{-15}
		Membrane	4.05×10^{-14}
		Vacuole	0.000112893
		Fungal-type cell wall	0.00657447
Overlap	Increased	Function ontology	
		Carnitine O-acetyltransferase activity	0.004722998
		Process ontology	
		Strand invasion	0.005073972
	Decreased	Process ontology	
		Vacuolar transport	3.08×10^{-11}
		Piecemeal microautophagy of nucleus	1.22×10^{-9}
		Autophagy	3.69×10^{-8}
		Cellular catabolic process	3.70×10^{-8}
		Protein targeting to vacuole	1.50×10^{-7}
		Microautophagy	1.58×10^{-7}
		Catabolic process	1.87×10^{-7}
		CVT pathway	3.92×10^{-6}
		Mitochondrion degradation	3.27×10^{-5}
		Macroautophagy	7.48×10^{-5}

(*continued*)

TABLE 2

(Continued)

Starvation condition	Relative abundance	GO term	*p*-value
		Chromatin modification	0.000224553
		Macromolecule catabolic process	0.000389849
		Chromatin organization	0.000451277
		Organelle organization	0.000617029
		Cellular macromolecule catabolic process	0.001004526
		Response to starvation	0.001575439
		Cellular response to nutrient levels	0.001891053
		Response to nutrient levels	0.00224056
		Cellular response to starvation	0.002809263
		Cellular response to extracellular stimulus	0.004995302
		Cellular response to external stimulus	0.004995302
		Post-translational protein modification	0.005010949
		Response to external stimulus	0.005630996
		Response to extracellular stimulus	0.005630996
		Late endosome to vacuole transport	0.008312095
		Component ontology	
		Mitochondrion	4.71×10^{-5}
		Protein complex	7.18×10^{-5}
		Cell part	7.35×10^{-5}
		Cell	7.74×10^{-5}
		Intracellular	0.00013285
		Mitochondrial envelope	0.000181034
		Intracellular part	0.000553794
		Mitochondrial membrane	0.000695522
		Membrane	0.000801977
		Organelle membrane	0.000808519
		Organelle envelope	0.00085302
		Envelope	0.00085302
		Preautophagosomal structure	0.000976079
		Membrane-bounded organelle	0.001284374
		Intracellular membrane-bounded organelle	0.001284374
		Mitochondrial part	0.001303991
		Cytoplasm	0.00207307
		Organelle	0.002665859
		Intracellular organelle	0.002665859
		Organelle inner membrane	0.00636321
		Membrane part	0.006585958
		Mitochondrial inner membrane	0.008489214

We tested genes for GO term enrichment that were significantly either increased or decreased in relative abundance in either experiment as determined using a regression model and an FDR of 5%. We also identified those genes that were significantly altered in relative abundance in both experiments. *P*-values are Bonferroni adjusted to account for multiple testing.

fermentable carbon sources have significantly reduced half-lives in both starvation regimes (Table S6). These data strongly implicate mitochondrial function as critical for survival in both of these nutrient starvations.

We found that genes annotated to peroxisome function have reduced half-lives when starved for phosphate (Figure 6A). By contrast and consistent with our analysis of relative death rates, mutants of peroxisomal genes result in increased absolute survival when cells are starved for leucine (Figure 6B). Peroxisomes are organelles that perform fatty acid oxidation and we have previously found that mRNAs related to peroxisome function are increased in expression at slow growth rates (Brauer *et al.* 2008). Although we found multiple lines of evidence for the role of oxidative metabolism in the starvation response, we did not find that gene sets defined by metabolic pathways are significantly altered in survival. In fact, lipid-linked oligosaccharide biosynthesis and inositol phosphate biosynthesis are the only nonrandomly distributed biosynthetic pathways in phosphate and leucine starvation, respectively (Table S6).

In agreement with our analysis of relative death rates, we identified significantly decreased survival of mutants annotated to the GO term autophagy (GO:0006914) in both phosphate (Figure 6C) and leucine (Figure 6D) starvation. Several of these mutants exhibit extremely rapid death upon nutrient starvation (Table S4 and Table S5), indicating that the autophagy pathway is critical for surviving nutrient starvation. We also

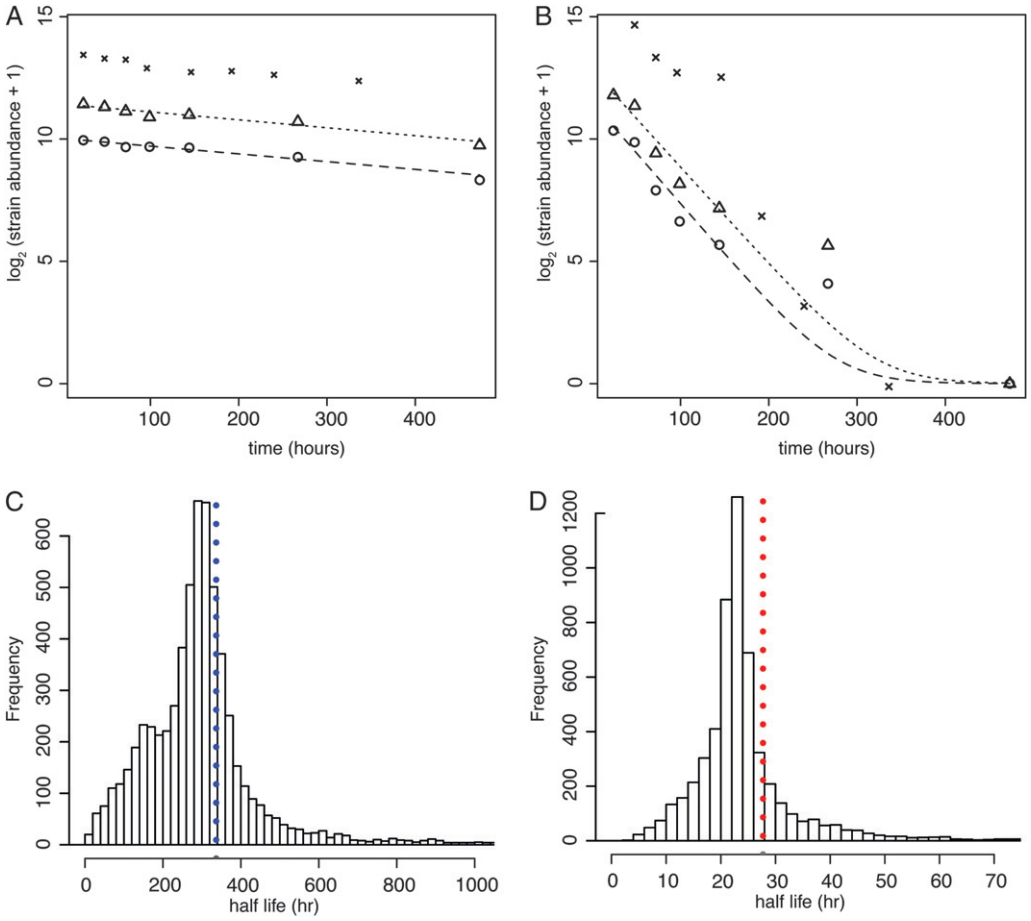

FIGURE 5.—Quantitative analysis of absolute death rates during prolonged starvation. We calculated the absolute rate of death for mutants using measurements of population viability and estimates of relative strain abundance using quantitative barcode sequencing of uptags (circles) and downtags (triangles) for the putatively neutral *HOΔ0* allele starved for phosphate (A) and leucine (B). The data presented are barcode counts normalized between all uptag or downtag sequencing results. A value of 1 was added to all normalized barcode counts prior to $\log_2$ transformation. The rate of death was determined using a generalized linear model for uptag (long-dashed line) and downtag (short-dashed line) data. These rates were compared to rates calculated from independent data (viable cells per microliter) obtained for the isogenic strain BY4742 (x's) subjected to starvation in pure cultures. We calculated death rates for all mutants in each starvation condition and converted these values to half-lives for all barcode data that yielded a significant death rate (FDR <5%). The distribution of half-lives for mutants starved for phosphate is centered around 289 hr (C) and 22.8 hr (D) for leucine-starved mutants. The half-life of the HOΔ0 strain when starved for phosphate (blue dotted line) or leucine (red dotted line) is shown for reference.

find that mutants in the GO term "translation" (GO:0006412) are enriched for significantly reduced half-lives in both phosphate (Figure 6C) and leucine (Figure 6D) starvations. This result contrasts with the apparent increased replicative life span of cells mutant for ribosomal functions (STEFFEN *et al.* 2008).

We found several cases in which gene sets are nonrandomly distributed in phosphate starvation only. In all cases these classes of mutants die faster than wild-type cells. These include mutants in mRNA processing (GO:0006397) and mRNA transport (GO:0051028), which have reduced survival in phosphate starvation (Figure 6E) but not in leucine starvation (Figure 6F). Similarly, mutants in gene sets related to chromatin functions including chromatin modification (GO:0016568) (Figure 6, G and H), the protein complexes histone acetyltransferase (Figure 6, G and H), and the histone deacetylase and Ino80 complex (Table S6); and mutants in the GO term cytoskeleton (GO:0005856) and GO Slim term microtubule organizing center (Figure 6, I and J) have reduced survival in phosphate starvation but not in leucine starvation. The different results for these gene classes suggest that just as some individual gene deletions have effects in only a single starvation condition, different genetic modules may be important for response to particular nutrient starvations.

We considered that slower growing mutants may have enhanced survival upon encountering starvation as slow growth rate is correlated with increased stress resistance (LU *et al.* 2009). Contrary to this possibility, we find that mutants that grow slowly in rich media laboratory conditions (GIAEVER *et al.* 2002) have greatly reduced half-lives when starved for phosphate (Figure 6K) and leucine (Figure 6L). Similarly, those mutants that are sensitive to rapamycin, an inhibitor of cell proliferation, have reduced half-lives in phosphate (Figure 6K) and leucine (Figure 6L) starvations. A similar result is observed for the ribosomal inhibitor, cycloheximide (Table S6). Mutants for genes that have been defined as phenotypic capacitors—*i.e.*, deletion of the gene results in increased variance of cell morphological traits (LEVY and SIEGAL 2008)—die faster, in phosphate starvation conditions (Table S6), perhaps indicating a require-

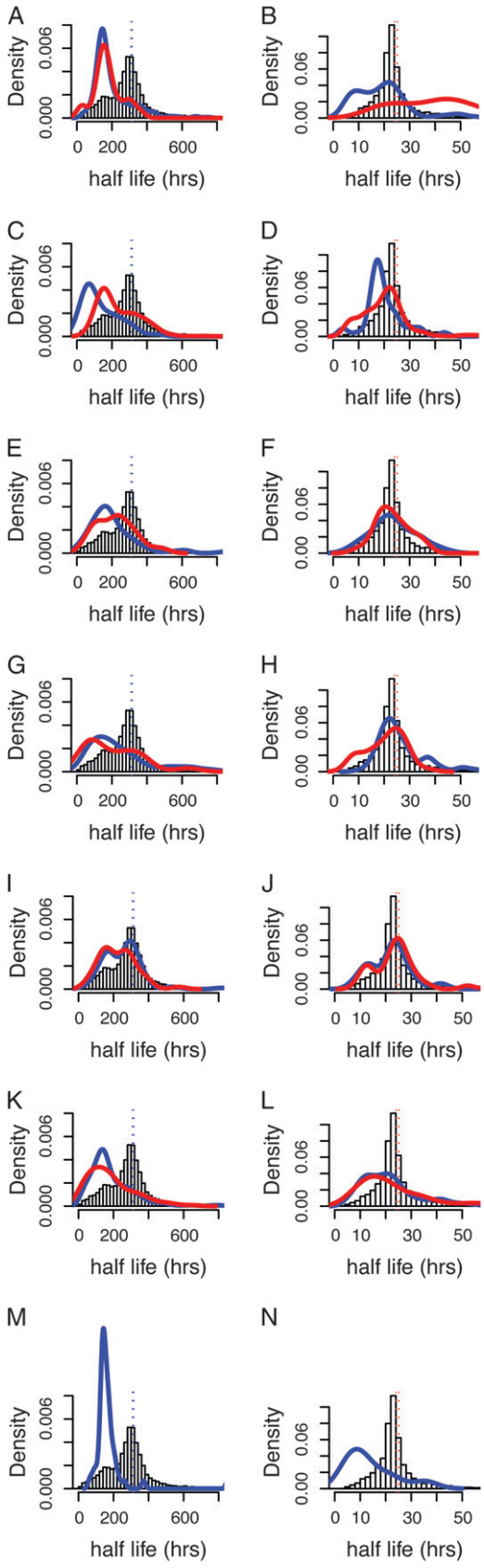

FIGURE 6.—Functional gene modules altering survival during nutrient starvation. The distributions of half-lives for subsets of genes defined by different methods of categorization were compared with the overall distribution of half-lives (white bars) in each experiment shown. (A) Phosphate starvation, mitochondrion organization (blue, Go Slim term, $n = 281$, $P = 5.88 \times 10^{-41}$) and peroxisome organization (red, GO:0007031, $n = 27$, $P = 0.00013$). (B) Leucine starvation, mitochondrion organization (blue, Go Slim term, $n = 276$, $P = 9.23 \times 10^{-14}$) and peroxisome organization (red, GO:0007031, $n = 25$, $P = 4.63 \times 10^{-5}$). (C) Phosphate starvation, autophagy (blue, GO:0006914, $n = 51$, $P = 2.0 \times 10^{-13}$) and translation (red, GO:0006412, $n = 305$, $P = 1.46 \times 10^{-12}$). (D) Leucine starvation, autophagy (blue, GO:0006914, $n = 50$, $P = 0.00014$) and translation (red, GO:0006412, $n = 301$, $P = 2.33 \times 10^{-11}$). (E) Phosphate starvation, mRNA processing (blue, GO:0006397, $n = 91$, $P = 3.38 \times 10^{-11}$) and mRNA transport (red, GO:0051028, $n = 42$, $P = 6.45 \times 10^{-5}$). (F) Leucine starvation, mRNA processing (blue, GO:0006397, $n = 91$, $P = 0.87$) and mRNA transport (red, GO:0051028, $n = 40$, $P = 0.87$). (G) Phosphate starvation, chromatin modification (blue, GO:0016568, $n = 89$, $P = 2.86 \times 10^{-6}$) and histone acetyltransferase complex (red, SGD-defined protein complex, $n = 41$, $P = 8.82 \times 10^{-5}$). (H) Leucine starvation, chromatin modification (blue, GO:0016568, $n = 90$, $P = 0.032$) and histone acetyltransferase complex (red, SGD-defined protein complex, $n = 40$, $P = 0.16$). (I) Phosphate starvation, cytoskeleton (blue, GO:0005856, $n = 151$, $P = 2.03 \times 10^{-5}$) and microtubule organizing center (red, SGD-defined protein complex, $n = 30$, $P = 3.16 \times 10^{-5}$). (J) Leucine starvation, cytoskeleton (blue, GO:0005856, $n = 148$, $P = 0.14$) and microtubule organizing center (red, SGD-defined protein complex, $n = 30$, $P = 0.75$). (K) Phosphate starvation, slow growth in YPD (blue, defined by Giaever *et al.* 2002, $n = 637$, $P = 2.46 \times 10^{-103}$) and impaired growth in rapamycin (red, defined by Dudley *et al.* 2005, $n = 137$, $P = 1.16 \times 10^{-19}$). (L) Leucine starvation, slow growth in YPD (blue, defined by Giaever *et al.* 2002, $n = 619$, $P = 3.04 \times 10^{-16}$) and impaired growth in rapamycin (red, defined by Dudley *et al.* 2005, $n = 132$, $P = 0.00058$). (M) Phosphate starvation, *MRPL10* cluster of the yeast metabolic cycle (blue, defined in Tu *et al.* 2005, $n = 54$, $P = 1.62 \times 10^{-16}$). (N) Leucine starvation, *MRPL10* cluster of the yeast metabolic cycle (blue, defined in Tu *et al.* 2005, $n = 53$, $P = 4.8 \times 10^{-6}$).

ment for phenotypic uniformity in the complex processes of cell cycle exit, aging, and survival.

Previously, we defined transcripts whose expression level is correlated with the growth rate of cells (Brauer *et al.* 2008). We found little evidence for altered survival conferred by null mutations in genes that encode growth rate-related transcripts (Table S6). Among gene sets defined by global gene expression studies we find that mutants corresponding to those transcripts expressed in the "reductive building" phase of the yeast metabolic cycle (Tu *et al.* 2005) are the only nonrandomly distributed gene set in our data and die faster than wild type in both phosphate (Figure 6M) and leucine (Figure 6N). These mRNAs primarily encode mitochondrial ribosomal components, making this observation consistent with our identification of mitochondrial function as critical for response to nutrient starvation.

DISCUSSION

The aim of this study was to determine the contribution of all nonessential genes to the processes of exit from the cell cycle and persistence in a viable state

during prolonged starvation. We developed an approach to multiplexed mutant analysis using quantitative sequencing of molecular barcodes to identify the relative abundance of gene deletion mutants in complex mixtures. We performed several control experiments to validate this method and identify the optimal experimental and analytical methods for analyses of these data. Importantly, we developed a statistical approach to analyzing barcode counts derived from high-throughput sequencing methods that is widely applicable. We demonstrate that statistically significant changes in relative mutant abundance within a complex mixture are determined using an overdispersed Poisson generalized linear model applied to time series data. When combined with accurate determination of population viability, our method enabled simultaneous analysis of the absolute rate of survival of ~4000 null mutants using a single culture. Estimation of *absolute* rates of mutant survival results in data that are comparable with individual mutant analysis and are therefore more biologically informative. We treated absolute survival during nutrient starvation as a quantitative trait and tested sets of genes for nonrandom distribution within the overall distribution enabling a system-level analysis of genetically defined modules that are active in the complex processes of cell cycle exit, aging, and survival during prolonged starvation.

Survival during nutrient starvation is a complex quantitative trait: We examined survival upon starvation in two vastly different scenarios. By starving yeast for phosphate we studied the response to a natural limitation. This is presumably a limitation that yeast cells experience in the wild and thus we can expect that genetic networks exist that mediate response to phosphate starvation. This condition is in contrast to our alternate starvation regime: starvation of a leucine auxotroph (*LEU2Δ0*) for leucine. This is an entirely laboratory-contrived scenario and we have no reason to expect that yeast cells should be able to respond appropriately to leucine starvation. Consistent with this expectation, we observe an order of magnitude difference in the rate of death when populations are starved for leucine compared with phosphate.

Despite the dramatically different selections imposed by these two starvation conditions we identified sets of genes that when mutated impair the response to starvation of both nutrients. We identified autophagy as a cellular process that when impaired results in reduced survival in both starvation conditions. This is consistent with the activation of autophagy by nutrient starvation (Takeshige *et al.* 1992) and its requirement for survival of diverse nutrient starvation conditions. The rapid rate with which autophagy mutants die suggests that this function is required at a very early stage following cell cycle exit and entry into quiescence. We also determined that strains mutant for mitochondrial functions are impaired in their response to starvation for phosphate and leucine. This is, to our knowledge, the first evidence that mitochondrial function is required for survival during phosphate and leucine starvations. Thus, whereas proliferative metabolism in yeast may typically involve fermentation, nonproliferative metabolism may generally require respirative metabolism even in the presence of abundant glucose.

We found genetic evidence for several additional processes that appear to be uniquely important in the case of phosphate starvation. These processes include those related to mRNA processing and transport, chromatin remodeling, and microtubule and cytoskeletal functions. These findings are consistent with previous studies of phosphate starvation. The transcriptional reprogramming of the cell associated with nutrient starvation (Gasch *et al.* 2000; Saldanha *et al.* 2004) is likely impaired in cells defective in mRNA-related processes, consistent with this finding. Regulation of the phosphate starvation response requires chromatin remodeling (Steger *et al.* 2003) at *PHO4*-regulated genes, which is consistent with our identification of significantly altered behavior of chromatin-remodeling mutants including the INO80 complex. Response to nutrient starvation is likely to involve reorganization of the cytoskeleton (Bauer *et al.* 1993; Lee *et al.* 1998), consistent with our identification of reduced survival of this class of mutants upon phosphate starvation.

An interpretation we favor is that mutants with increased survival upon leucine starvation represent cases of genetic suppression and are informative about genes whose functions must be downregulated to ensure successful cell cycle arrest and initiation of a survival program in response to natural starvations. A good example of this is the increased survival upon leucine starvation that is conferred by loss of *TOR1* function. We suggest that the suppression of leucine-starvation lethality by *TOR1* deletion mimics the required downregulation of the TOR1 system when nutrition is insufficient. We posit that leucine insufficiency is not detected by the intact TOR system, and thus cells starved for leucine continue to attempt growth even while starving and thereby kill themselves. We identified several additional mutants that confer increased survival upon starvation for leucine. These mutants are potentially informative about additional gene functions that must be downregulated upon natural starvations.

Conversely, mutants that reduce survival of leucine-starved cells can be considered cases of genetic enhancement and are informative about genes whose function must be increased during normal cell cycle arrest and survival. These mutants largely overlap with mutants that reduce survival upon phosphate starvation.

Previous studies of chronological aging in yeast may be influenced by starvation for auxotrophic requirements: Yeast is a useful model system for studying aging

at a cellular level. The literature in this field is notable for the widespread disagreement between researchers regarding which genes and processes are relevant for either chronological or replicative aging. Our study suggests that some of these discrepancies may be due to a failure to control for the critical relationship between genotype and nutrient limitation. This study reinforces our previous report showing that the first nutrient exhausted in the culture profoundly affects the survival of cells (Boer *et al.* 2008). Here we have shown that the effect of each null mutation on the death rate differs as a function of which nutrient is depleted first in the media. It has long been known that yeast cells are able to maintain high viability for many hundreds of days when prototrophs are starved for different nutrients (Lillie and Pringle 1980) and the comparatively short life span reported for yeast cells under starvation conditions in different studies (Fabrizio *et al.* 2001, 2005; Longo 2003; Powers *et al.* 2006; Steffen *et al.* 2008; Wei *et al.* 2008; Burtner *et al.* 2009) is in clear conflict with these earlier observations. Recently, two articles described a similar study to our report in which the entire yeast mutant library was starved in a pooled experiment and assayed using DNA microarrays to determine the abundance of each molecular barcode (Fabrizio *et al.* 2010; Matecic *et al.* 2010). In the study by Matecic *et al.* (2010) cells were starved in complete media with either 2% or 0.5% glucose. In the former case, the half-life of the wild-type strain is ~3 days whereas 0.5% glucose results in a half-life of ~10–11 days. In the study by Fabrizio *et al.* (2010) cells were starved in synthetic complete media and the heterogeneous population appears to have a half-life of ~3–4 days. As with many studies of "chronological aging," these studies made use of strains bearing auxotrophic markers and for which the limiting nutrient (*i.e.*, the nutrient that is first exhausted in the culture) is undefined. Given our previous results (Boer *et al.* 2008) and the results of this study, it is likely that a careful determination of which nutrient starvation is first experienced by cells would do much to reconcile conflicting observations in the literature.

It also seems possible that the different responses to natural and unnatural nutrient depletion may underlie some of the discrepancies reported in studies of replicative aging in yeast. In particular, we suggest that the use of low concentrations of glucose as a model for "caloric restriction" (Lin *et al.* 2002; Kaeberlein *et al.* 2005a; Murakami *et al.* 2008) may be confounded by the fact that different concentrations of glucose may alter which nutrient is first exhausted in these media.

The use of auxotrophic strains may affect many studies: Given the profound impact that auxotrophies have on the survival of mutants upon starvation, and the potential unappreciated effect this may have had in many aging studies, we believe that extreme caution should be employed for physiological studies that make use of auxotrophic markers in undefined media. Auxotrophies have been found to confound other genetic studies (Destruelle *et al.* 1995; Chopra *et al.* 1999) and it seems probable that confusion due to their use may be more pervasive than we expect. Given that the growth rate of chemically complemented strains differs from that of an otherwise isogenic prototrophic strain (Pronk 2002) and transporters of auxotrophic requirements, such as the uracil permease, are degraded under starvation conditions for nutrients other than uracil (Volland *et al.* 1994), it seems possible that auxotrophies may generally affect assays that rely on either growth rate or viability in a variety of experimental designs.

Implications for complex genetic traits: The classification of heritable phenotypes often entails a subjective division between mutant and nonmutant classes. In reality, all traits exist on a quantitative continuum and our distinction between mutant and nonmutant phenotypes represent an arbitrary, but practical, distinction. Quantitative trait mapping in crosses of genetically diverged strains provides a means of identifying the genetic basis of traits (Brem *et al.* 2002; Rockman and Kruglyak 2006) but these efforts are informative only when genes are polymorphic and the results detect only alleles of strong effect. Ideally, a comprehensive genetic approach to quantitative variation should identify all genes contributing to phenotypic variation and describe their effect size. We achieved this in our experiment—albeit, for null alleles only—by treating survival of nutrient starvation as a quantitative trait and carefully controlling the environment and genotype. The product of this experimental design is a high-resolution, and near complete, quantitative phenotype–genotype map.

A central question in quantitative genetics is how many genes underlie complex traits. We have shown that several hundred genes (*i.e.*, a large fraction of the genome) can contribute to phenotypic variation in response to nutrient starvation. We find it plausible that a similar relationship holds in complex human traits, *i.e.*, that many hundreds of genes are likely to contribute to complex trait variation such as morphological variation or disease risk. This is consistent with the small amount of genetic variance explained in genetic studies of complex traits such as human height (Weedon *et al.* 2008) and risk for schizophrenia (International Schizophrenia Consortium 2009). The possible contribution to phenotypic variation of many hundreds of genes may be an underlying source of the hidden heritability problem in human genetic studies (Manolio *et al.* 2009). The additional complexity contributed by allelic variation, evolution, population history, and environmental variation makes the genetic dissection of complex traits in any natural population a formidable task.

We thank Jessica Buckles and Donna Storton for technical assistance with Illumina Sequencing. This research was supported by the National Institute of General Medical Sciences Center for Quantitative

Biology (GM 071508), National Institutes of Health grants to D.B. (GM 046406) and J.S. (HG 002913), and startup funds from New York University to D.G.

LITERATURE CITED

Bauer, F., M. Urdaci, M. Aigle and M. Crouzet, 1993 Alteration of a yeast SH3 protein leads to conditional viability with defects in cytoskeletal and budding patterns. Mol. Cell. Biol. **13:** 5070–5084.

Boer, V. M., S. Amini and D. Botstein, 2008 Influence of genotype and nutrition on survival and metabolism of starving yeast. Proc. Natl. Acad. Sci. USA **105:** 6930–6935.

Boer, V. M., C. A. Crutchfield, P. H. Bradley, D. Botstein and J. D. Rabinowitz, 2010 Growth-limiting intracellular metabolites in yeast growing under diverse nutrient limitations. Mol. Biol. Cell **21:** 198–211.

Boyle, E. I., S. Weng, J. Gollub, H. Jin, D. Botstein *et al.*, 2004 GO:TermFinder—open source software for accessing Gene Ontology information and finding significantly enriched Gene Ontology terms associated with a list of genes. Bioinformatics **20:** 3710–3715.

Brauer, M. J., A. J. Saldanha, K. Dolinski and D. Botstein, 2005 Homeostatic adjustment and metabolic remodeling in glucose-limited yeast cultures. Mol. Biol. Cell **16:** 2503–2517.

Brauer, M. J., J. Yuan, B. D. Bennett, W. Lu, E. Kimball *et al.*, 2006 Conservation of the metabolomic response to starvation across two divergent microbes. Proc. Natl. Acad. Sci. USA **103:** 19302–19307.

Brauer, M. J., C. Huttenhower, E. M. Airoldi, R. Rosenstein, J. C. Matese *et al.*, 2008 Coordination of growth rate, cell cycle, stress response, and metabolic activity in yeast. Mol. Biol. Cell **19:** 352–367.

Brem, R. B., G. Yvert, R. Clinton and L. Kruglyak, 2002 Genetic dissection of transcriptional regulation in budding yeast. Science **296:** 752–755.

Burtner, C. R., C. J. Murakami, B. K. Kennedy and M. Kaeberlein, 2009 A molecular mechanism of chronological aging in yeast. Cell Cycle **8:** 1256–1270.

Chopra, R., V. M. Sharma and K. Ganesan, 1999 Elevated growth of Saccharomyces cerevisiae ATH1 null mutants on glucose is an artifact of nonmatching auxotrophies of mutant and reference strains. Appl. Environ. Microbiol. **65:** 2267–2268.

de Hoon, M. J. L., S. Imoto, J. Nolan and S. Miyano, 2004 Open source clustering software. Bioinformatics **20:** 1453–1454.

Destruelle, M., H. Holzer and D. J. Klionsky, 1995 Isolation and characterization of a novel yeast gene, ATH1, that is required for vacuolar acid trehalase activity. Yeast **11:** 1015–1025.

Dudley, A. M., D. M. Janse, A. Tanay, R. Shamir and G. M. Church, 2005 A global view of pleiotropy and phenotypically derived gene function in yeast. Mol. Syst. Biol. **1:** 2005.0001.

Fabrizio, P., and V. D. Longo, 2003 The chronological life span of Saccharomyces cerevisiae. Aging Cell **2:** 73–81.

Fabrizio, P., F. Pozza, S. D. Pletcher, C. M. Gendron and V. D. Longo, 2001 Regulation of longevity and stress resistance by Sch9 in yeast. Science **292:** 288–290.

Fabrizio, P., C. Gattazzo, L. Battistella, M. Wei, C. Cheng *et al.*, 2005 Sir2 blocks extreme life-span extension. Cell **123:** 655–667.

Fabrizio, P., S. Hoon, M. Shamalnasab, A. Galbani, M. Wei *et al.*, 2010 Genome-wide screen in Saccharomyces cerevisiae identifies vacuolar protein sorting, autophagy, biosynthetic, and tRNA methylation genes involved in life span regulation. PLoS Genet. **6:** e1001024.

Gasch, A. P., P. T. Spellman, C. M. Kao, O. Carmel-Harel, M. B. Eisen *et al.*, 2000 Genomic expression programs in the response of yeast cells to environmental changes. Mol. Biol. Cell **11:** 4241–4257.

Giaever, G., A. M. Chu, L. Ni, C. Connelly, L. Riles *et al.*, 2002 Functional profiling of the Saccharomyces cerevisiae genome. Nature **418:** 387–391.

Gray, J. V., G. A. Petsko, G. C. Johnston, D. Ringe, R. A. Singer *et al.*, 2004 "Sleeping beauty": quiescence in Saccharomyces cerevisiae. Microbiol. Mol. Biol. Rev. **68:** 187–206.

Hartwell, L. H., 1991 Twenty-five years of cell cycle genetics. Genetics **129:** 975–980.

Hartwell, L. H., 2002 Nobel Lecture. Yeast and cancer. Biosci. Rep. **22:** 373–394.

Hartwell, L. H., J. Culotti, J. R. Pringle and B. J. Reid, 1974 Genetic control of the cell division cycle in yeast. Science **183:** 46–51.

Ho, C. H., L. Magtanong, S. L. Barker, D. Gresham, S. Nishimura *et al.*, 2009 A molecular barcoded yeast ORF library enables mode-of-action analysis of bioactive compounds. Nat. Biotechnol. **27:** 369–377.

International Schizophrenia Consortium, 2009 Common polygenic variation contributes to risk of schizophrenia and bipolar disorder. Nature **460:** 748–752.

Johnston, G. C., J. R. Pringle and L. H. Hartwell, 1977 Coordination of growth with cell division in the yeast Saccharomyces cerevisiae. Exp. Cell Res. **105:** 79–98.

Kaeberlein, M., D. Hu, E. O. Kerr, M. Tsuchiya, E. A. Westman *et al.*, 2005a Increased life span due to calorie restriction in respiratory-deficient yeast. PLoS Genet. **1:** e69.

Kaeberlein, M., R. W. Powers, K. K. Steffen, E. A. Westman, D. Hu *et al.*, 2005b Regulation of yeast replicative life span by TOR and Sch9 in response to nutrients. Science **310:** 1193–1196.

Lee, J., K. Colwill, V. Aneliunas, C. Tennyson, L. Moore *et al.*, 1998 Interaction of yeast Rvs167 and Pho85 cyclin-dependent kinase complexes may link the cell cycle to the actin cytoskeleton. Curr. Biol. **8:** 1310–1321.

Levy, S. F., and M. L. Siegal, 2008 Network hubs buffer environmental variation in Saccharomyces cerevisiae. PLoS Biol. **6:** e264.

Lillie, S. H., and J. R. Pringle, 1980 Reserve carbohydrate metabolism in Saccharomyces cerevisiae: responses to nutrient limitation. J. Bacteriol. **143:** 1384–1394.

Lin, S.-J., M. Kaeberlein, A. A. Andalis, L. A. Sturtz, P.-A. Defossez *et al.*, 2002 Calorie restriction extends Saccharomyces cerevisiae lifespan by increasing respiration. Nature **418:** 344–348.

Longo, V. D., 2003 The Ras and Sch9 pathways regulate stress resistance and longevity. Exp. Gerontol. **38:** 807–811.

Lu, C., M. J. Brauer and D. Botstein, 2009 Slow growth induces heat-shock resistance in normal and respiratory-deficient yeast. Mol. Biol. Cell **20:** 891–903.

Manolio, T. A., F. S. Collins, N. J. Cox, D. B. Goldstein, L. A. Hindorff *et al.*, 2009 Finding the missing heritability of complex diseases. Nature **461:** 747–753.

Matecic, M., D. L. Smith, X. Pan, N. Maqani, S. Bekiranov *et al.*, 2010 A microarray-based genetic screen for yeast chronological aging factors. PLoS Genet. **6:** e1000921.

Murakami, C. J., C. R. Burtner, B. K. Kennedy and M. Kaeberlein, 2008 A method for high-throughput quantitative analysis of yeast chronological life span. J. Gerontol. A Biol. Sci. Med. Sci. **63:** 113–121.

Nurse, P., 1975 Genetic control of cell size at cell division in yeast. Nature **256:** 547–551.

Nurse, P., Y. Masui and L. Hartwell, 1998 Understanding the cell cycle. Nat. Med. **4:** 1103–1106.

Nurse, P. M., 2002 Nobel Lecture. Cyclin dependent kinases and cell cycle control. Biosci. Rep. **22:** 487–499.

Pierce, S. E., R. W. Davis, C. Nislow and G. Giaever, 2007 Genome-wide analysis of barcoded Saccharomyces cerevisiae gene-deletion mutants in pooled cultures. Nat. Protoc. **2:** 2958–2974.

Powers, R. W., M. Kaeberlein, S. D. Caldwell, B. K. Kennedy and S. Fields, 2006 Extension of chronological life span in yeast by decreased TOR pathway signaling. Genes Dev. **20:** 174–184.

Pronk, J. T., 2002 Auxotrophic yeast strains in fundamental and applied research. Appl. Environ. Microbiol. **68:** 2095–2100.

Rockman, M. V., and L. Kruglyak, 2006 Genetics of global gene expression. Nat. Rev. Genet. **7:** 862–872.

Saldanha, A. J., 2004 Java Treeview—extensible visualization of microarray data. Bioinformatics **20:** 3246–3248.

Saldanha, A. J., M. J. Brauer and D. Botstein, 2004 Nutritional homeostasis in batch and steady-state culture of yeast. Mol. Biol. Cell **15:** 4089–4104.

Smith, A. M., L. E. Heisler, J. Mellor, F. Kaper, M. J. Thompson *et al.*, 2009 Quantitative phenotyping via deep barcode sequencing. Genome Res. **19:** 1836–1842.

Steffen, K. K., V. L. MacKay, E. O. Kerr, M. Tsuchiya, D. Hu *et al.*, 2008 Yeast life span extension by depletion of 60s ribosomal subunits is mediated by Gcn4. Cell **133:** 292–302.

Steger, D. J., E. S. Haswell, A. L. Miller, S. R. Wente and E. K. O'Shea, 2003 Regulation of chromatin remodeling by inositol polyphosphates. Science **299:** 114–116.

Storey, J. D., and R. Tibshirani, 2003 Statistical significance for genomewide studies. Proc. Natl. Acad. Sci. USA **100:** 9440–9445.

Takeshige, K., M. Baba, S. Tsuboi, T. Noda and Y. Ohsumi, 1992 Autophagy in yeast demonstrated with proteinase-deficient mutants and conditions for its induction. J. Cell Biol. **119:** 301–311.

Tu, B. P., A. Kudlicki, M. Rowicka and S. L. McKnight, 2005 Logic of the yeast metabolic cycle: temporal compartmentalization of cellular processes. Science **310:** 1152–1158.

Volland, C., D. Urban-Grimal, G. Géraud and R. Haguenauer-Tsapis, 1994 Endocytosis and degradation of the yeast uracil permease under adverse conditions. J. Biol. Chem. **269:** 9833–9841.

Weedon, M. N., H. Lango, C. M. Lindgren, C. Wallace, D. M. Evans *et al.*, 2008 Genome-wide association analysis identifies 20 loci that influence adult height. Nat .Genet. **40:** 575–583.

Wei, M., P. Fabrizio, J. Hu, H. Ge, C. Cheng *et al.*, 2008 Life span extension by calorie restriction depends on Rim15 and transcription factors downstream of Ras/PKA, Tor, and Sch9. PLoS Genet. **4:** e13.

Werner-Washburne, M., E. Braun, G. C. Johnston and R. A. Singer, 1993 Stationary phase in the yeast Saccharomyces cerevisiae. Microbiol. Rev. **57:** 383–401.

Yan, Z., M. Costanzo, L. E. Heisler, J. Paw, F. Kaper *et al.*, 2008 Yeast barcoders: a chemogenomic application of a universal donor-strain collection carrying bar-code identifiers. Nat. Methods **5:** 719–725.

Zaman, S., S. I. Lippman, X. Zhao and J. R. Broach, 2008 How Saccharomyces responds to nutrients. Annu. Rev. Genet. **42:** 27–81.

Communicating editor: B. J. Andrews

GENETICS

Supporting Information
http://www.genetics.org/cgi/content/full/genetics.110.120766/DC1

System-Level Analysis of Genes and Functions Affecting Survival During Nutrient Starvation in *Saccharomyces cerevisiae*

David Gresham, Viktor M. Boer, Amy Caudy, Naomi Ziv, Nathan J. Brandt, John D. Storey and David Botstein

DOI: 10.1534/genetics.110.120766

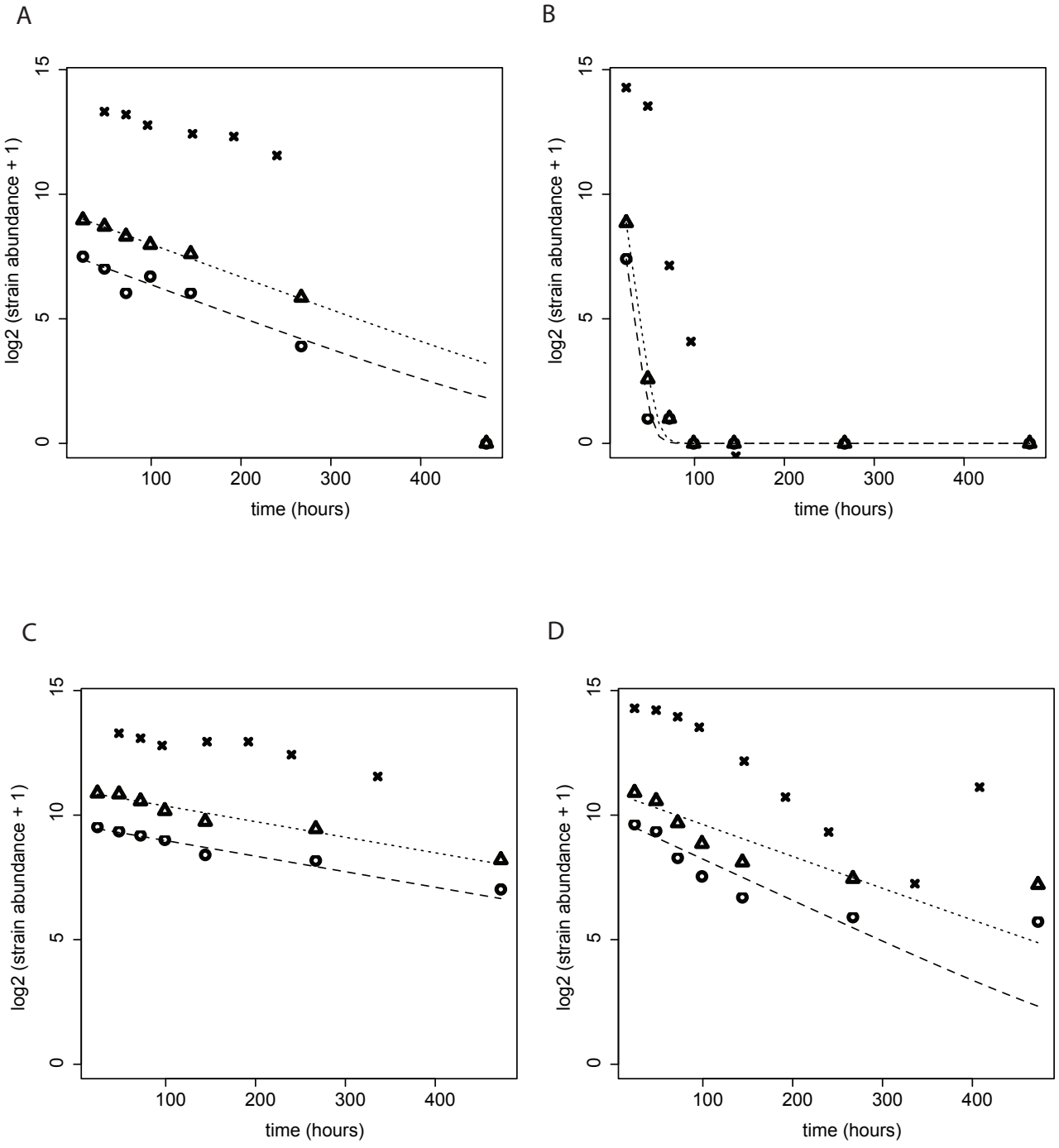

FIGURE S1.—Comparison of absolute death rate estimates inferred from pooled experiment for uptags (circles) and downtags (triangles) with individual mutant analysis in pure cultures (crosses). Data are presented for *ATG10Δ0* starved for (A) phosphate and (B) leucine and *PEX13Δ0* starved for (C) phosphate and (D) leucine. Barcode counts are the normalized as described in (methods). Pure culture counts are number of viable cells/μL.

TABLE S1

Summary of all barcode sequencing experiments

Expt.	Experiment Description	Figure	Total Reads	Uptags	Dntags	Unmapped
1	Single barcode	Figure 2A	2,340,984	2,340,984	n/a	n/a
2	VB_s_1	Figure 2C	4,277,717	2,124459 (49.7%)	2,153,258 (50.3%)	1,155,131 (27.0%)
3	PCR 30 cycles	Figure 2B	3,585,742	552,455 (15.4%)	3,033,287 (84.6%)	998,506 (27.8%)
4	PCR 25 cycles	Figure 2B	7,737,553	3,477,644 (44.9%)	4,259,909 (55.0%)	1,970,333 (25.5%)
5	PCR 20 cycles	Figure 2B	3,659,194	1,532,589 (41.9%)	2,126,605 (58.1%)	900,199 (24.6%)
6	PCR 15 cycles	Figure 2B	1,029,015	657,650 (63.9%)	371,365 (36.21%)	253,044 (24.6%)
7	VB_s_1_repeat	Figure 2C	7,594,300	2,793,694 (36.8%)	4,800,606 (63.2%)	1,908,887 (25.1%)
8	Unselected pool 1	Figures 2D, 4 and 5	8,185,598	2,134,658 (26.1%)	6,050,940 (73.9%)	1935672 (23.6%)
9	Unselected pool 2	Figures 2D, 4 and 5	7,457,342	1,431,691 (19.2%)	6,025,651 (80.8%)	1786893 (24.0%)
10	Phosphate starvation t = 0hr	Figures 4 and 5	7,360,688	1,821,104 (24.7%)	5,539,584 (75.2%)	2,044,378 (27.8%)
11	Phosphate starvation t = 24hr	Figures 4 and 5	7,969,303	2,463,639 (30.9%)	5,505,664 (69.1%)	2,172,916 (27.3%)
12	Phosphate starvation t = 48hr	Figures 4 and 5	7,740,944	2,383,718 (30.8%)	5,357,226 (69.3%)	1,904,457 (24.6%)
13	Phosphate starvation t = 72hr	Figures 4 and 5	6,201,163	2,114,157 (34.1%)	4,087,006 (65.9%)	1,509,900 (24.3%)
14	Phosphate starvation t = 99hr	Figures 4 and 5	6,552,758	1,321,294 (20.2%)	5,231,464 (79.8%)	1,623,590 (24.8%)
15	Phosphate starvation t = 144hr	Figures 4 and 5	8,331,886	3,714,888 (44.6%)	4,616,998 (55.4%)	2,030,725 (24.4%)
16	Phosphate starvation t = 267hr	Figures 4 and 5	8,977,470	1,555,925 (17.3%)	7,421,545 (82.7%)	2,531,095 (28.2%)
17	Phosphate starvation t = 473hr	Figures 4 and 5	4,815,151	1,029,621 (21.4%)	3,785,530 (78.6%)	1,165,598 (24.2%)
18	Leucine starvation t = 0hr	Figures 4 and 5	8,367,434	2,347,434 (28.0%)	6,020,000 (71.9%)	2,041,278 (24.4%)
19	Leucine starvation t = 24hr	Figures 4 and 5	8,822,841	2,330,193 (26.4%)	6,492,648 (73.6%)	2,155,783 (24.4%)
20	Leucine starvation t = 48hr	Figures 4 and 5	9,494,929	3,845,443 (40.5%)	5,649,486 (59.5%)	2,342,985 (24.7%)
21	Leucine starvation t = 72hr	Figures 4 and 5	7,512,308	2,243,459 (29.9%)	5,268,849 (70.1%)	1,853,548 (24.7%)
22	Leucine starvation t = 99hr	Figures 4 and 5	8,884,437	2,217,260 (25.0%)	6,667,177 (75.0%)	2,215,985 (24.9%)
23	Leucine starvation t = 144hr	Figures 4 and 5	8,383,630	2,486,648 (29.7%)	5,896,982 (70.3%)	2,107,793 (25.1%)
24	Leucine starvation t = 267hr	Figures 4 and 5	8,711,905	1,579,689 (18.1%)	7,132,216 (81.9%)	2,427,867 (27.9%)
25	Leucine starvation t = 473hr	Figures 4 and 5	8,644,145	1,779,999 (20.6%)	6,864,146 (79.4%)	2,938,915 (34.0%)

TABLES S2-S6

Tables S2-S6 are available for download as Excel files at http://www.genetics.org/cgi/content/full/genetics.110.120766/DC1.

TABLE S2: Modeled relative survival rates for all mutants starved for phosphate.

We performed regression analysis for 6,806 barcodes corresponding to 4,337 unique genes. We determined that 1,333 genes behave significantly differently than the overall population at an FDR of 5%.

TABLE S3: Modeled relative survival rates for all mutants starved for leucine.

We performed regression analysis for 6,740 barcodes corresponding to 4299 unique genes. We determined that 3,951 genes behave significantly differently than the overall population at an FDR of 5%.

TABLE S4: Modeled absolute survival rates for all mutants starved for phosphate.

We performed regression analysis for 6,806 barcodes corresponding to 4,337 unique genes. We calculated significant absolute death rates for 4,143 genes at an FDR of 5%.

TABLE S5: Modeled absolute survival rates for all mutants starved for leucine.

We performed regression analysis for 6,730 barcodes corresponding to 4,239 unique genes. We calculated significant absolute death rates for 3,591 genes at an FDR of 5%.

TABLE S6: Complete results for gene class enrichment analysis.

We tested gene classes defined by GO terms, GO slim terms, protein complexes, biochemical pathways, high throughput phenotypic studies and gene expression studies for significant non-random distributions of half lives.